ABSTRACT

LEE, KYOUNG OOK. Coaxial Atmospheric Pressure Plasma Discharge for Treatment of Filaments and Yarns. (Under the direction of Mohamed A. Bourham.)

Characteristics of non-thermal atmospheric-pressure plasma generated in a coaxial cylindrical Dielectric-Barrier Discharge (DBD) were investigated for application in treatment of polymer and 100% un-mercerized cotton yarns. The discharge characteristics were investigated by measuring the electrical parameters and utilization of developed plasma circuit models to obtain plasma electron temperature, number density and the electron-neutral collision frequency. The experiments were conducted in helium and oxygenated helium plasma in absence and presence of yarns. The discharge is capacitively-coupled and is induced by an audio-frequency, 4.5 kHz, oscillating voltage. The electrical voltage-current (V-I) characteristics optimized for plasma processing, by the oxygen and helium flow rate ratio, was found to be about 40sccm for oxygen flow. Optical emission spectroscopy (OES) was used to determine the plasma composition and to evaluate plasma temperature and number density. The plasma electron number density decreased from 2.2×10^{16} to 1.4×10^{16} per cubic meter when oxygen flow rate was increased to 100sccm in a 10,000sccm helium flow, while the electron temperature increased from 0.15 to 0.4 eV for the same increase in oxygen flow rate. It was also found that the plasma experiences some streamers and that the streamer's electron temperature has a wide range between 0.5 to 2 eV. The optimized oxygen flow rate for polymer yarn processing was found to be 40sccm in a 10,000sccm helium flow.

Coaxial Atmospheric Pressure Plasma Discharge
for Treatment of Filaments and Yarns

by
Kyoung Ook Lee

A thesis submitted to the Graduate Faculty of
North Carolina State University
in partial fulfillment of the
requirements for the Degree of
Master of Science

Nuclear Engineering

Raleigh, North Carolina

2007

APPROVED BY:

_____   _____
    O.E. Hankins   K. Weingner

_____
Mohamed A. Bourham
Chair of Advisory Committee

DEDICATION

I dedicate this thesis to my father, the late Dae-Hyun Lee passed away in

May of 2005 and to my family; my mother, my wife and loving son Julian.

BIOGRAPHY

Kyoung Lee was born in Seoul, Korea, on May 21, 1975. He graduated with a Bachelor of Science in Physics. Following his BS graduation he was enrolled in Yosei University in Seoul, South Korea, studying Applied Physics. He was admitted to the graduate program at North Carolina State University in August 2005 in the Department of Nuclear Engineering to study plasma physics and fusion energy.

ACKNOWLEGEMENTS

TABLE OF CONTENTS

LIST OF TABLES

LIST OF FIGURES

Chapter 1

Introduction

Most atmospheric pressure plasmas are non-thermal and depart from equilibrium, such plasmas have been studied for a variety of materials processing and surface modification techniques [1-5]. Atmospheric pressure plasma discharge has more advantages over low pressure plasma discharges, which operate under vacuum and thus require vacuum systems, pressure gauges, vacuum controllers, gate valves, special metal-seal flanges, and other expensive equipment. However, vacuum plasmas are easily generated at considerably moderate voltages while electrical discharges at atmospheric pressure are, usually, more difficult to generate at low voltages [6]. At atmospheric pressure the mean free path for electrons is short and the generated plasma is highly collisional, and hence the required breakdown voltage is typically in the kilovolts range.

The breakdown condition in atmospheric pressure discharges may cause unstable formation of the discharge, which appears in the form of streamers and filamentary discharges, and may occasionally happen in dielectric barrier discharges (DBD) [1-3, 6]. Many atmospheric pressure plasma sources were designed with features to enhance the electrical efficiency for plasma generation. The structure of parallel-plate capacitive discharge has been widely used to perform material processing and surface functionalization in many applications such as plasma oxidation, etching, plasma enhanced chemical vapor deposition, surface decontamination and sterilization, etc. [1-9].

The plasma device in this research is a coaxial cylindrical discharge using the theory of dielectric-barrier discharge (DBD) at audio-frequency ranges (4 – 12 kHz). The central

electrode is insulated inside a ceramic, or glass, tube and the generated electric field has a cylindrical symmetry. The discharge condition is determined by the conditions that occur between the electrodes such as the geometry and formation of the plasma sheath around the central electrode, and by the effect of the gas mixture and the respective flow rates. The secondary emission process, typically in DC glow discharges, is an essential process through which the discharge is self-sustained, however, this process is not the same in a dielectric barrier discharge since the electric field oscillates and thus the charge transfer is via conduction and displacement currents. The characteristics of plasma are presented by the First Townsend's coefficient (α) and the secondary electron-emission coefficient (γ). These transitions can be distinguished in dielectric barrier discharges, such as the configuration of the device described in this thesis in which the Pyrex glass tube acts as the dielectric and is enclosed inside of an outer aluminum mesh that acts as the ground electrode. Dielectric barrier discharges (DBD) may cause unstable discharges appearing in the form of streamers or filamentary discharges; however, an advantage of the DBD is the prevention of arc formation in the discharge. Additionally, DBD can generate plasma at higher pressures, such as atmospheric, which is favorable for textile industry. In general, DBD sources are efficient in many material processing techniques at atmospheric pressure in which streamers are minimized and stable plasma can be obtained; hence, material surface damage could be eliminated and electrical power transfer to the plasma can be maximized [2,6,8].

In this work, an equivalent circuit model was used to obtain the electron number density from the measured electrical parameters of the discharge. The model is based on equivalent RLC circuit for the plasma in concentric cylindrical discharge driven by an oscillating voltage at audio frequency of 4.5 kHz. The recorded voltage and current, in real-

time, are used to obtain plasma parameters, in real-time, which allows for a better understanding of the nature of the discharge and its effectiveness on the treatment of yarns and filaments. The experimental arrangement was not intended to investigate geometric size effect of the plasma source but to investigate the effectiveness of the discharge on surface modifications of yarns and filaments; however, a plasma model was investigated for optimization of the electrical efficiency to obtain a stable discharge at atmospheric pressure. Optimization includes investigation of the optimum levels of mixing oxygen with helium in the discharge, electric power density and operating frequency; all such parameters are adjustable for optimization of device efficiency. Optical emission spectroscopy (OES) was used to obtain plasma number density and temperature in presence of polymer yarns treated in He/O gas mixture discharges. Plasma temperature and density measurements from OES were compared to results obtained from a model that uses an equivalent circuit model.

The plasma treatment with a mixture of oxygen at a gas flow rate of 40sccm in 10,000sccm helium has shown improvement in the properties of the treated yarns such as wettability, adhesion, lubricity, heat resistance, cohesive strength of filaments, breaking strength, hydrophilicity and/or hydrophobicity. In this research surface chemical and physical composition of plasma treated yarns were investigated. Scanning electron microscopy (SEM) was used to provide information on surface morphology of the treated polymers, and Energy Dispersive Spectrometry (EDS) determines the surface composition.

LITERATURE REVIEW

1.1 Cylindrical Capacitively-Coupled RF Discharge

In concentric electrodes plasma discharge induced by radio frequency voltage the electrical potential in the space between the cylindrical electrodes is instantaneously induced according to the following potential equation:

$$\phi = \frac{V_0 e^{-i\omega t}}{\ln(b/a)} \ln(b/r)$$

where a and b are the radii of the inner and outer electrodes, respectively, and $\omega = 2\pi f$ is the angular frequency of applied voltage which has an amplitude V_o. When such very high voltage V_o is supplied to the electrodes with a certain gas filling in between, the atoms and molecules of the gas or gas mixture are electrically decomposed, an electron-ion pair is formed, and an electric current flows through the discharge causing the breakdown condition. Such breakdown potential depends on the types of electrode materials, the distance between them, the density of the gas, and the extent of ionization. Fig. 1 shows the voltage drop, self DC bias [10] and formation of the plasma potential.
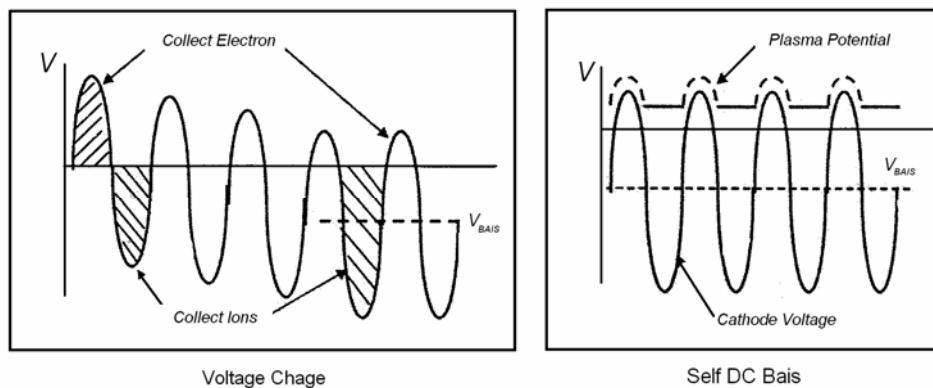
Figure 1 Plasma voltage drop and Self DC Bias [10]

.

The plasma potential is usually small compared to the cathode fall potential, cathode drop, and thus ions are accelerated towards the cathode due to the strong voltage across the sheath, which upon impact on the cathode surface causes sputtering of the cathode and deposition of sputtered atoms. The self DC bias is a result of the negative potential on the cathode, and the generation of plasma is then determined by the self bias voltage.

In any RF discharge the electrical field change due to plasma potential characterizes the discharge and the formation of the oscillating sheathes. Electrons and ions are accelerated through the sheath region as the sheath changes its polarity following the RF frequency change, however, most of the ions respond to the time-average changes in the sheath while electrons respond to instantaneous changes [6, 11]. Thus, the change in the electrons kinetic energy is instantaneous, and electrons gain kinetic energy on the expenses of the sheath potential. The major factor in self-sustaining the discharge is the secondary electron emission occurring from the cathode due to ion impact. The current inside of the cathode sheath is caused by the ionization of the secondary electrons accelerated by the strong electric field developed across the sheath. Electrons emitted from the cathode are accelerated by the electric field and will induce ionization of the surrounding gas due to collision with neutral atoms/molecules. The discharge can be self-sustained as long as a proper voltage usually less than the breakdown voltage is kept applied on the electrodes [6]. At higher pressures, the discharge is highly collisional, which is typical for atmospheric pressure discharges, and the production of secondary electron emission is no longer the mechanism by which a self-sustained condition is achieved unless the discharge is a DC discharge at very high voltage applied on the electrodes.

1.2 The First Townsend's coefficient (α) and the secondary electron-emission coefficient (γ) mode at atmospheric pressure

RF discharges could be initiated in different types of gases to induce pseudo glow discharge, or a corona discharge; however, the Dielectric barrier discharge (DBD) is different in the mechanism by which the discharge is initiated. In a DBD, the current flowing through the insulators is displacement when the sheath is fully expanded on one side, and is conductive when the sheath is fully shrink at the other side. In general, the RF discharge mode is close to the regimes of DC discharge from the point of current-voltage relation. The first Townsend's coefficient α and the secondary electron-emission coefficient γ in RF discharges have been investigated in the literature [12, 13]. Figure 2 shows the voltage-current characteristics of traditional DC glow discharge. Normal and abnormal glow regimes are the most useful operating regimes of glow discharges and the discharge is mainly characterized by the first Townsend coefficient α. After transition from the α mode to the γ mode the corona discharge takes place.
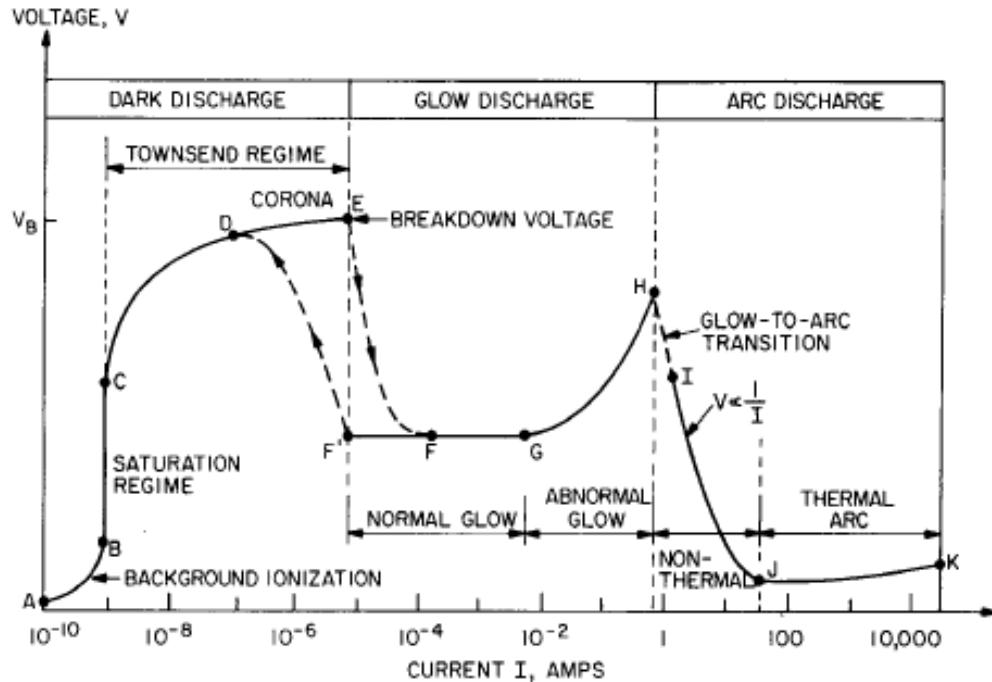
Figure 2 Voltage-current characteristics of DC glow discharge [10]

After an electron avalanches and collides with surrounding gas molecules, the gas gets ionized and plasma is formed. The First Townsend coefficient α is a strong function of ionization energy ε_{iz}, electron mean free path λ_e, and the electric field E, and is expressed in the following form

$$\alpha = \frac{Const.}{\lambda_e} \exp(-\frac{\varepsilon_{iz}}{E\lambda_e})$$

where the electron mean-free path is given by $\lambda_e = \frac{1}{\sigma n} = \frac{kT}{\sigma P}$, which is the mean free path for inelastic (mainly ionization) electron-neutral collisions, $E\lambda_e$ is a typical electron energy gain in the field between collisions [6, 11]. Recognizing that the mean-free path is inversely proportional to the pressure $\lambda_e \propto \frac{1}{p}$ then α equation can be re-written in the form

$$\frac{\alpha}{p} = A\exp(-Bp/E_{RF})$$

7

, where A and B are determined experimentally and found to be constant over a restricted range of E/p for any given gas, and the electric field E is replaced by the RF electric field E_{RF}.

The secondary electron emission, γ, or the second Townsend's coefficient results from ion impact on the cathode. The relation of α, γ mode is an equation that defines the first and second Townsend coefficients and has the form $\alpha d = \ln\left(1 + \dfrac{1}{\gamma}\right)$.

This equation is valid for DC and AC discharges as it relates the two coefficients in the discharge to each other, even for discharges with less secondary electron emission. Combining the cylindrical electric field equation and setting the breakdown RF electric field as the negative gradient of the voltage $E_{RF} = -\nabla\phi = \dfrac{V_{RF}}{d_{eff}\,\ln(b/a)}$, then the $\dfrac{\alpha}{p}$ relation will

be $\dfrac{\alpha}{p} = A\exp(-Bp\,/\,\dfrac{V_{RF}}{d\,\ln(b/a)})$.

Solving above equation for the amplitude of the RF voltage $\widetilde{V}_{RF}$, which is the RF breakdown

voltage, one gets $\widetilde{V}_{RF} = \dfrac{Bpd_{eff}\,\ln(b/a)}{\ln(Apd_{eff}\,\ln(b/a)) - \ln\left[\ln(1+\gamma^{-1})\right]}$

, where A and B are the same constants in the self-sustained condition. Here it is clear that the voltage necessary for gas breakdown, $\widetilde{V}_{RF}$ depends on the pressure, the electrodes effective gap distance, d_{eff} and the dimensions $\ln(b/a)$ of the coaxial discharge in which the inner and outer radii are a and b, respectively [6, 11]. This breakdown condition is typical to that of a DC glow discharge and only differs in having the amplitude of the RF voltage

instead of the DC voltage, and the effect of the coaxial geometry as opposed to the traditional parallel planer electrodes in DC discharges.

1.3 Dielectric Barrier Discharge at Atmospheric Pressure

A Dielectric Barrier Discharge (DBD) is a non-equilibrium non-thermal atmospheric pressure discharge in which short-lived finite plasma filaments appear over the surface of the electrodes [14,15]. The discharge may also be characterized as a collection of streamers or random microdischarge with spatial-temporal behavior and thus it is viewed as a nonequilibrium plasma state. The DBD discharges at atmospheric pressure are widely used for surface modifications of polymers and textile materials to make chemical reaction on the surface, typically oxidation that leads to enhanced wettability and adhesion [16]. It is also used to provide surface activation for further plasma processes such as implantation and grafting of antimicrobial and insect repelling agents into fabrics [17]. DBD discharges may be manufactured in various configurations such as planer electrodes, or coaxial geometry. Figure 3 shows various forms of DBD discharges in which one electrode is embedded inside the dielectric barrier (top left drawing), coaxial with interior barrier (top right drawing), both electrodes are embedded in the insulating barriers (bottom left drawing), single barrier in the middle of the discharge (bottom middle drawing, or side-by-side electrodes with one common barrier (bottom right drawing).

9
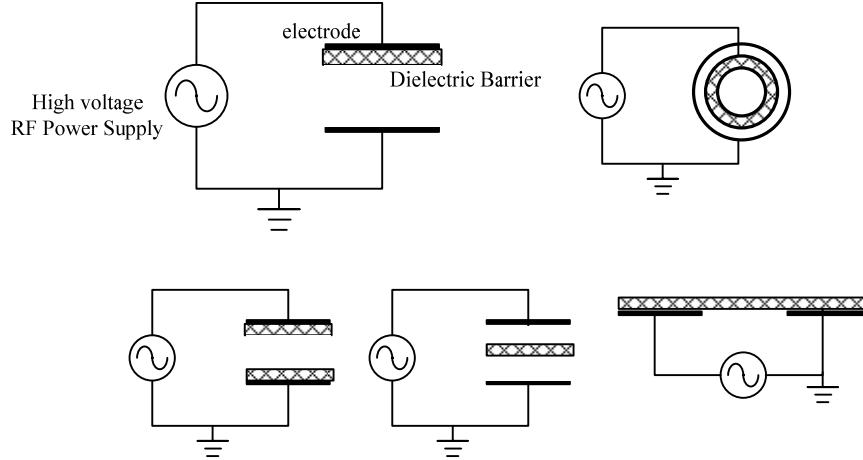
Figure 3 Illustration of various DBD discharge configurations

An atmospheric pressure RF glow discharge could be formed when large number of electrons exists at the beginning of each half cycle, and the electrons are produced from Penning ionization [1,6]. The electron population is inversely proportional to the electric field, and the dielectric barrier material plays a key role in the discharge. The DBD discharges operate with oscillating electric field at low 4-15kHz or high 13.54MHz frequencies in which the displacement current $\varepsilon_o \dfrac{\partial E}{\partial t}$ plays the main role in the flow of electric current in the discharge. The dielectric barrier may be fabricated from plastics, glass, ceramics or enamels. The microdischarges are generated by accumulating charges on the dielectric and thus forming a conductive layer that allows for the conduction of current and hence induces the breakdown of the working gas and causes ionization. When streamers are formed and touch the electrodes, some of the surface charges are neutralized and the streamers are disrupted such that the discharge can occur periodically as a result of streamers interruption in the plasma volume between the barrier-covered electrodes.

1.4 Plasma Treatment and Processing of Cotton

Cotton is the purest natural form of cellulose made up of anhydroglucose units containing a basic repeating polymer chain structure [18]. Figure 4 shows the cellulose polymer structure of a chemical compound in cotton in which OH groups. Cotton, by nature, is a hydrophilic fiber and the high degree of moisture content is partially due to water being attracted to the numerous hydroxyl groups.
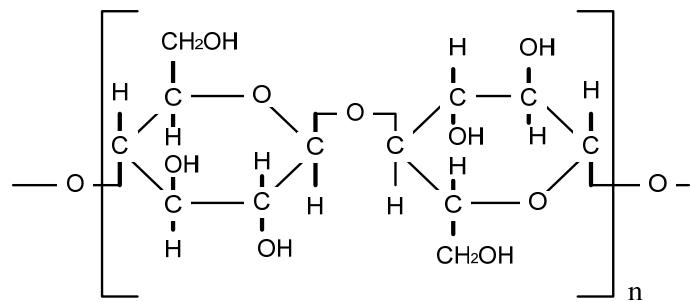
Figure 4 Cellulose polymer structural formula of a chemical compound in Cotton [18]

Numerous researches has been conducted on treatment and processing of cotton using plasma techniques, among which are the use of DBD discharges [19-21]. It has been shown that DBD discharges are efficient in providing surface modifications of cotton, as well as other textile materials, which include enhanced wettability, grafting and inclusion of insect repelling compounds [22-27]. The coaxial DBD plasma device, which operates at atmospheric pressure, provides interaction between the plasma active species and cotton yarns. These species are electrons, ions, excited atoms (radicals), and UV radiation. Other important plasma processes takes place in the device, such as recombination, diffusion and

atomic line radiation. Figure 4 shows a schematic of the coaxial plasma device and the corresponding plasma formation including the possible plasma species available in the discharge. The fiber, or yarn, passes through the plasma and is exposed to various processes depending on the plasma gas in use; these processes may be deposition, etching, scission, cross-linking or diffusion and implantation.
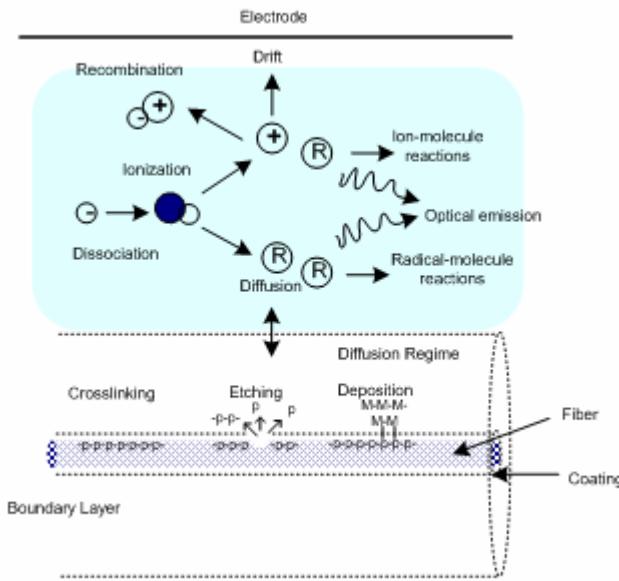
Figure 5 Illustration of plasma reaction mechanisms in coaxial DBD discharge for treatment of fiber

Etching would be induced when using active plasma gases such as oxygen, carbon tetrafluoride, carbon hexafluoride, argon, or halogen-based gases. Reaction of such active gases with the surface of the yarn produces volatile byproducts and causes thin-layer etching. Other surface modifications such as surface roughness can be caused by oxygen gas in plasma processing [20, 28, 29]. Using oxygen provides oxide surface cleaning, increases wettability, and improves adhesion   Cross linking takes place when radicals (or excited species) react within the surface and forming chemical bonds, which results in cross-linked

surface between the radicals and the open chain in the surface chemical structure. Plasma-induced cross linking employs the use of inert gases such as argon or helium to remove some atomic species from the surface, and generates reactive surface radicals; inclusion of reactive gases such as oxygen, CF_4 or C_3F_6 enhances the cross-linking process [28, 30]. Table 1 summarizes some of the well-known interactions between plasma species and surfaces, showing the effect of both low and high ion bombardment in the plasma [30, 31].

Table 1 Typical plasma gas interaction with surface

	Inert Gas Plasma	Reactive Gas Plasma
Low ion bombardment	Plasma cleaning	Plasma oxidation Surface activation Surface hardening Polymerization
High ion bombardment	Sputtering Sputter etching	Reactive sputter Etching

Chapter 2

Experimental

2.1 Atmospheric Pressure Coaxial Plasma Discharge Design

The plasma device was designed in coaxial geometry in which the glass cylinder acts as the dielectric and an outer aluminum mesh serves as the ground electrode. An inner electrode is placed on the axis of the discharge cylinder and can either be positively or negatively charged. The device was designed to operate at atmospheric pressure in a DBD configuration to provide various treatments of filaments and yarns in a static or continuous exposure to plasma. Various working gases can be used in this device with helium serving as the seed gas, mixed with a fraction of other gases of interest such as oxygen or fluorocarbons. The discharge is induced via a 4-15 kHz audio-frequency power supply circuit in which two out-of-phase transformers supply the necessary voltage to the discharge electrodes. The device has various controls for voltage, plasma working gases and mixing ratio, gas flow rates, and operating frequency. The device allows for exposure of the samples, yarns and filament, either on stationary or dynamic regimes, thus one can characterize the effect of exposure for extended time or the dynamic exposure in fast throughput. Figure 5 illustrates the structure of the coaxial DBD discharge "Coaxial Atmospheric Pressure RF Discharge (CAPRFD)", in which the central electrode is serves as the anode and the outer aluminum mesh serves as the grounded electrode, the glass tube is the DBD for this design.
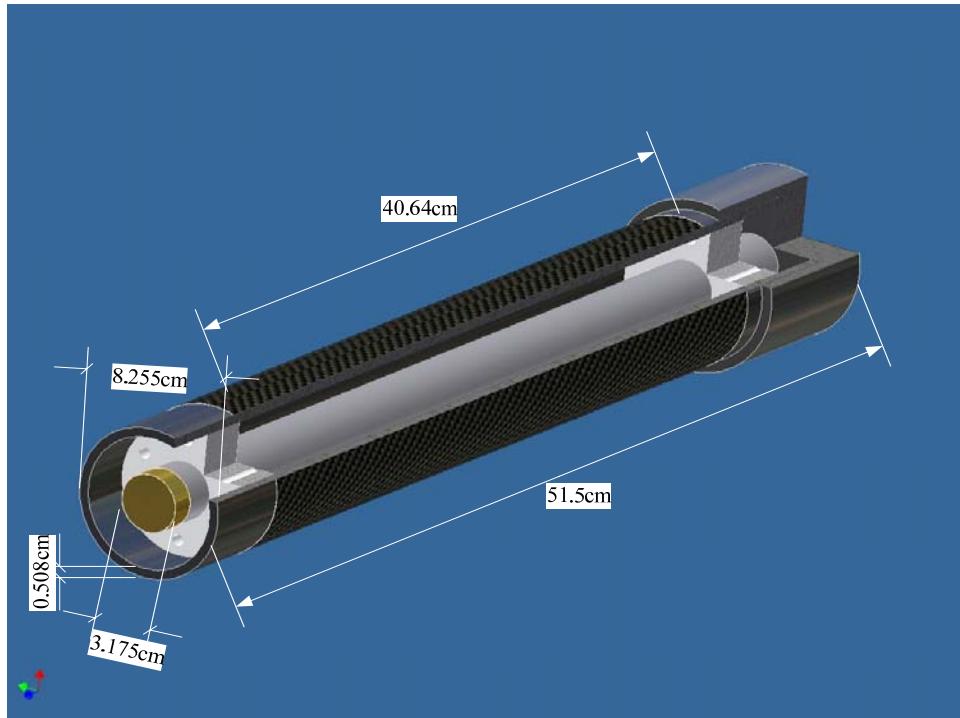
Figure 6 Coaxial Atmospheric Pressure RF discharge (CAPRFD) device

The coaxial cylindrical geometry has an advantage in plasma treatment of filament and yarn materials by passing the filament/yarn through the interior of the glass chamber under controlled gas flow rates and residence time. The power supply is coupled to two out-of-phase transformers for voltage doubling across the electrodes, and the frequency could be adjusted between 4-15kHz for best tuning between the power supply and the plasma. The inner electrode is a 3.175cm aluminum rod, and the Pyrex glass tube serves as the dielectric barrier. The Pyrex tube is enclosed by an outer aluminum mesh, which serves as the ground electrode. End flanges are made of Teflon, which supports the inner electrode, has inlets for gas flow and has inlets to pass yarns and filaments from one end to the other end through the plasma. Helium is used as the seed gas in the DBD discharge mode and oxygen is mixed into the helium at specific ratio to generate oxygenated helium plasma. The DBD discharges can,

15

in general, produce streamers and may also be considered as corona discharges when operated at atmospheric pressure, however, the device is designed to operate in a micro-discharges mode with less streamers to reduce coronal and streamers damage to the exposed filaments/yarns.

2.2 Experimental Setup and Procedure

As previously described in section 2.1, the experimental device is composed of a Pyrex glass tube serving as the plasma chamber, gas flow controllers for helium and oxygen (other gases could also be used), an audio-frequency (AF) power supply with out-of-phase output transformers, and electrical and plasma diagnostics. Figure 6 illustrates the experimental setup showing the power supply connection to the coaxial electrodes, the gas manifolds, and the optical emission spectroscopy setup. In this geometry the gas flows only in one direction, which is the direction of yarn/filament for continuous feed through the plasma. Samples were exposed to helium and oxygenated-helium plasma in a stationary exposure for 5 minutes at a fixed electric field frequency of 4.5 kHz. Real time electrical (voltage and current) and optical emission spectroscopy data were recorded. The discharge voltage is measured via a Tektronix P6015A, 1:1000, 3.0pF, 100 MHz compensated capacitively-coupled high voltage probe, and the current is measured by a Pearson (model 2877) current monitor.. A 4-channel digital oscilloscope, Tektronix TDS-224, 100 MHz, 1 Giga Sample/sec, is used for real-time recording of the current and voltage.
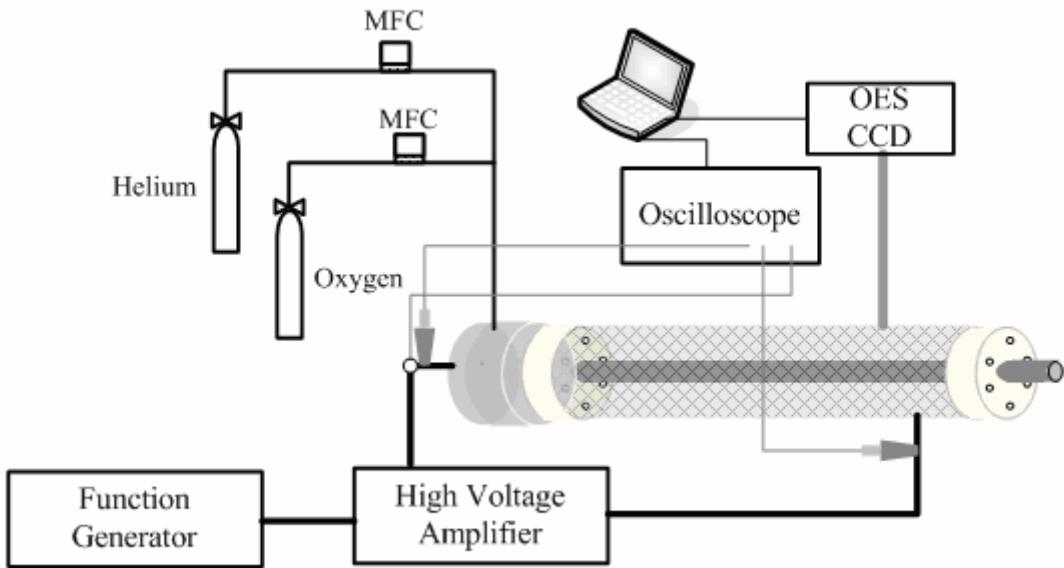
Figure 7 Schematic of the experimental setup

High purity 99.95% helium and oxygen gases are used, the gas flow rates are determined by the setting of each mass flow controller (MFC-MKS 247) to control the mixing ratio between helium and oxygen. Experiments were conducted using four different oxygen ratios in the helium flow, these ratios are determined by the flow rate of oxygen in a constant helium flow of 10,000sccm; the flow rates of oxygen were 23sccm, 43sccm, 64sccm, 84sccm and 100scc. The plasma is generated in the annular space and filaments/yarns are placed inside the discharge then removed after exposure, the samples are weighed pre and post exposure and optical microscopy pictures were obtained.

Optical emission spectroscopy (OES) measurements have been performed to analyze of the emitted lines to obtain plasma temperature, density and composition. Spectral data were obtained using two Ocean Optics HR2000 fixed grating spectrometers. Both spectrometers are fitted with a 600 line/mm grating, 25μm slit and Ocean Optics L2 internal lens to focus the light onto the charge-coupled device (CCD). The grating of the UV-VIS

spectrometer is blazed at 500 nm and views the wavelengths between 300 nm and 736 nm. The VIS-NIR spectrometer has a range of 600 nm to 1025 nm with the grating blazed at 750 nm. The spectrometers are power calibrated using an Ocean Optics LS-1-CAL lamp. Spectral data are transferred from the spectrometers to a PC via IEEE interface card and an Ocean Optics software package (SpectraSuite Spectrometer Operating Software). Collected spectral data are analyzed using PeakFit spectra package to determine the emission, and/or absorption lines, line identification and plasma composition.

Chapter 3

Theory and Analysis Methods

3.1 Plasma Model from Electrical Measurements

Electrical measurements of the discharge voltage and current are used in a plasma model to determine the plasma parameters such as plasma electron number density n_e, electron plasma temperature T_e, and electron-neutral collision frequency v_m. A plasma model for the discharge was developed based on the assumption that the discharge can be modeled as a coaxial capacitor in which the plasma dielectric constant plays the main role in determining the nature of the discharge. Figure 8 illustrates the coaxial discharge with a dual signal generator as the driving potential, and the plasma equivalent electric circuit for the plasma impedance and capacitance.
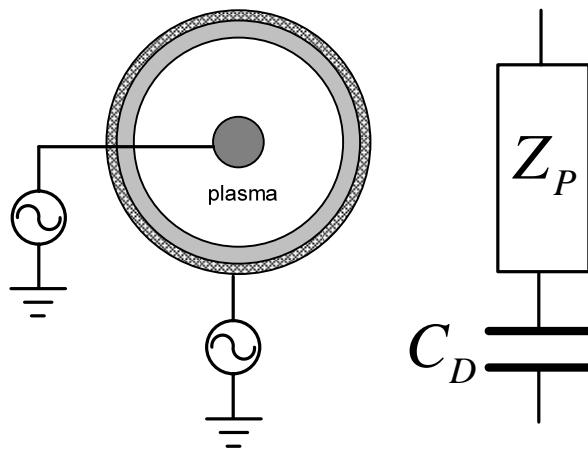
Figure 8 Coaxial DBD plasma discharge with dual signal generators and the equivalent impedance and capacitance

The plasma electrical circuit model uses the measured voltage and current to determine the system admittance in real time, and a solver provides a solution to the plasma

permittivity to obtain plasma electron number density and the electron-neutral collision frequency. The discharge current for this low-frequency, LF, discharge, is given by $I_{LF}(t) = \tilde{I}_{LF} e^{j\omega t + \delta}$, where $\omega = 2\pi f$ is the angular frequency at which the power supply provides the discharge voltage and current, and δ is the phase angle between the voltage and current. The voltage across the anode and cathode is given by $V_{LF}(t) = \tilde{V}_{LF} e^{j\omega t}$, and both voltage and current are continuously monitored in real time and recorded on the digital oscilloscope. The capacitance of the coaxial DBD system, C_D, is simplified to the capacitance of a cylindrical geometry, like a coaxial cable, and is then given by

$$C_D = 2\pi\varepsilon_o k_d \frac{L}{\ell n(c/b)} ,$$ where ε_D is the chamber permittivity and is equal to $\varepsilon_D = \varepsilon_o k_d$ in which $\varepsilon_0 = 8.854 \times 10^{-12} C^2 / N^2 m^2$ is the permittivity of free space and k_d is the dielectric constant of the pyrex glass (= 4.7); b and c are the inner and outer electrode diameters, respectively.

The admittance of plasma, Y_P can be presented as the sum of the plasma conductance $\frac{1}{R_p}$, plasma inductive reactance $\frac{1}{j\omega L_p}$ and the vacuum capacitive reactance $j\omega C_0$, and hence the total admittance is given by $Y_p = \frac{1}{R_p} + \frac{1}{j\omega L_p} + j\omega C_0$. This admittance is the parallel combination of the series L_p and R_p with the cylindrical space capacitance C_0. The plasma resistance is related to the plasma inductance via the electron-neutarl collision frequency v_m as $R_p = v_m L_p$, and the plasma inductance is related to the vacuum capacitance through the resonance frequency, which is the electron plasma frequency $L_p = 1/\omega_{pe}^2 C_o$, where the

electron plasma frequency is given by $\omega_{pe} = \left(e^2 n_e / \varepsilon_o m\right)^{1/2}$ [6,10]. As the chamber is coaxial,

then the capacitance is taken for the cylindrical geometry as $C_0 = 2\pi\varepsilon_0 \dfrac{L}{\ell n(b/a)}$, where

$a < b$, and a is the diameter of the inner electrode and b is diameter of the dielectric barrier,

which is the discharge chamber's outer diameter.

Excluding the sheath from the admittance model, assuming only lumped circuit

elements of the plasma and vacuum capacitance, the admittance is then given by $Y = \dfrac{\tilde{I}_{LF}}{\tilde{V}_{LF}} e^{j\delta}$,

which can also be written as:

$$Y = \frac{\dfrac{C_0 e^2 n_e}{m_e \varepsilon_o v_m}}{\left(\dfrac{C_0 e^2 n_e}{m_e \varepsilon_o v_m}\right)^2 + \left(-\dfrac{C_0 e^2 n_e}{m_e \varepsilon_o \omega} + C_0 \omega\right)^2} + j\left(C_D \omega + \frac{\dfrac{C_0 e^2 n_e}{m_e \varepsilon_o v_m} - C_0 \omega}{\left(\dfrac{C_0 e^2 n_e}{m_e \varepsilon_o v_m}\right)^2 + \left(-\dfrac{C_0 e^2 n_e}{m_e \varepsilon_o \omega} + C_0 \omega\right)^2}\right)$$

This admittance equation incorporates the substitution of plasma resistance, inductance and

vacuum capacitance, and the electron plasma frequency. Hence, this equation could be used

to obtain the plasma density and the collision frequency based on the measured voltage and

current.

Rearranging in terms of the real and imaginary parts:

The real part: $\dfrac{\tilde{I}_{LF}}{\tilde{V}_{LF}} \cos\delta = \dfrac{\dfrac{C_0 e^2 n_e}{m_e \varepsilon_o v_m}}{\left(\dfrac{C_0 e^2 n_e}{m_e \varepsilon_o v_m}\right)^2 + \left(-\dfrac{C_0 e^2 n_e}{m_e \varepsilon_o \omega} + C_0 \omega\right)^2}$

The imaginary part: $\dfrac{\tilde{I}_{LF}}{\tilde{V}_{LF}}\sin\delta = C_D\omega + \dfrac{\dfrac{C_0 e^2 n_e}{m_e \varepsilon_o \nu_m} - C_0\omega}{\left(\dfrac{C_0 e^2 n_e}{m_e \varepsilon_o \nu_m}\right)^2 + \left(-\dfrac{C_0 e^2 n_e}{m_e \varepsilon_o \omega} + C_0\omega\right)^2}$

The solution of these equations yields an equation for the plasma electron number density and another equation for the electron-neutral collision frequency as follow:

$$n_e = \frac{m_e \varepsilon_o \omega \nu_m}{e^2}\frac{C_D C_0 \omega^2 - 1 - AC_0\omega\sin\delta}{C_D C_0 \nu_m \omega - AC_0(\omega\cos\delta + \nu_m\sin\delta)}$$

$$\nu_m = \omega\left(1 - 2C_D C_0 \omega^2\right)\tan\delta + \frac{\omega^2\left\{A^2 C_0 + C_D(C_D C_0 \omega^2 - 1)\right\}}{A\cos\delta}$$

These two equations, as derived from the electrical circuit model, provide a measure of the electron number density and the collision frequency in real time through measurement of discharge voltage and current.

3.2 Optical Emission Spectroscopy (OES)

Optical emission spectroscopy (OES) is an excellent plasma diagnostic technique to determine plasma species in the discharge, as well as obtaining plasma electron temperature T_e and electron number density n_e.

The intensity of an emitted spectral line is given by $I_{mn} = A_{mn} g_n N \dfrac{E_m - E_n}{Q} e^{-\frac{E_m}{kT_e}}$,

where

A_{mn} = transition probability (sec^{-1})

E_m & E_n = upper and lower level state energies (Joule)

g_n = statistical weight of upper state

N = species particle density (m^{-3})

T_e = electron temperature (^{O}K)

Q = partition function

From which the electron temperature is given by $kT_e = \dfrac{E_{m1} - E_{m2}}{ln\left(\dfrac{I_2 \lambda_2^3}{I_1 \lambda_1^3} \dfrac{g_1 f_1}{g_2 f_2}\right)}$, where f is the

oscillator strength at given wavelength λ [32].

For plasmas in local thermodynamic equilibrium (LTE), the relative line technique using the ratios of atomic, ionic, or molecular line intensities determines the kinetic temperature. The method relies on generating a Boltzmann plot using the relative line method: $ln\left(\dfrac{\lambda I}{gA}\right) = C - \dfrac{E_u}{kT_e}$, where λ is the wavelength, I is the relative intensity, g the statistical weight of the upper level, A the transition probability, E_u the energy of the upper level, k is Boltzmann's constant, T_e the plasma electron kinetic temperature, and C is a constant. The temperature of the plasma is determined from the slope of a line constructed from the Boltzmann factor, $ln\left(\dfrac{\lambda I}{gA}\right)$ versus the upper level energy E_u.

For high pressure discharges, the plasma usually departs from LTE, and thus the relative intensity method may not be used, instead the continuum of radiation is emitted from the discharge and a neutral bremmstrahlung method would be employed. Such discharges are dominated by electron-neutral collisions over electron-ion collisions.

In a discharge when hydrogen is present, even as a small fraction, the broadening of the H$_\alpha$ line is used to obtain the electron number density. Thus, using H$_\alpha$ line and

determining the line broadening, one can obtain the number density. The FWHM of Stark broadening is given by: $w_s = 2.5 \times 10^{-10} \alpha_{nn} (n_e, T_e) n_e^{3/2}$, where α_{nn} is the reduced wavelength ($\Delta\lambda / E_o$) and n_e in cm^{-3} and $\Delta\lambda = 2W \times n_e \times 10^{-16} + 3.5A \left(n_e \times 10^{-16} \right)^{1/4}$, where A is the ion-broadening parameter, and could be neglected for non hydrogen plasmas. The nominal density from measured width: $n_e = \left(\frac{FWHM_{true}}{w_{measured}} \right) \times 10^{23} \ m^{-3}$.

Although the coaxial discharge is atmospheric, i.e. high pressure discharge, however, an estimate of the plasma temperature using relative method and a Boltzmann plot could be obtained. The electron density and temperature obtained from OES can allow for a comparison between OES calculations and circuit model results. Results of both OES and circuit model can be used together to develop a more accurate model. It was assumed that the non-equilibrium DBD plasma in atmospheric pressure discharges may possess local thermodynamic equilibrium (LTE). Therefore, the Boltzmann plot and Stark broadening data are compared with results of circuit model for electron density and temperature in the helium and oxygenated helium coaxial discharge.

As plasma is composed of electrons, ions, and neutral particles; the plasma can maintain thermal equilibrium following Saha ionization equation and the Boltzmann distribution. However, the thermal equilibrium of the coaxial discharge experiment is not complete, i.e. complete thermodynamic equilibrium (CTE) does not exist, and the plasma departs from CTE. Photons, in particular, are not generated in the plasma chamber and thus interactions by photons don't reach equilibrium. Accordingly, a Local Thermodynamic Equilibrium (LTE) may be considered), in which more electrons are comparatively available than the case of CTE because the reaction with atoms, electrons and photons due to collisions is at lower rates.

Plasmas under LTE state are assumed to have an energy density that follows the Boltzmann distribution in which the particle distribution is derived from the Boltzmann distribution for energies. The Boltzmann plot method is a simple method assuming the plasma is at LTE [32]. The emitted intensity, as previously discussed, is given by:

$$\varepsilon_{ul} = \frac{1}{4\pi} A_{ul} \cdot n \cdot h\nu_{ul} \frac{g}{Z} \exp\left(-\frac{E_{iu}}{kT}\right)$$

, where n is the number of molecules at equilibrium temperature T, in a state i which has energy E_i and degeneracy g_i, N is the total number of molecules in the system and k is the Boltzmann constant. Using the Boltzmann plot method the above equation can be written as:

$$\ln\left(\frac{\varepsilon_{ul}\lambda}{n \cdot \nu_{ul} g}\right) = -\frac{E_{iu}}{kT} + K$$

where $K = \ln(hn / 4\pi Z)$. In the above equation K is a constant and will not affect the plot. All the parameters in K are independent of the line observed on the plot.

Two Ocean Optics HR2000 fixed grating spectrometers are available for use to obtain the spectra of the microwave discharge during coating process. Both spectrometers are fitted with a 600 line/mm grating, 25μm slit and Ocean Optics L2 internal lens to focus the light onto the CCD. The grating of the UV-VIS spectrometer is blazed at 500 nm and views the wavelengths between 300 nm and 736 nm. The VIS-NIR spectrometer has a range of 600 nm to 1025 nm with the grating blazed at 750 nm. The spectrometers are power calibrated using an Ocean Optics LS-1-CAL lamp. Spectral data are transferred from the two spectrometers to a PC via IEEE interface card and an Ocean Optics software package. Collected spectral data will be analyzed using PeakFit spectra package to determine the emission, and/or absorption lines. Plasma composition will be determined and plasma parameters can be obtained.

3.3 Material Characterization Techniques

Scanning electron microscopy (SEM) using a Hitachi variable pressure S-3200 system to obtain micrographs of the samples exposed to plasma. Energy Dispersive X-ray Spectroscopy (EDS) was used in conjunction with SEM to determine the elemental composition of the samples pre and post exposure to plasma.

Chapter 4

Results and Discussion

4.1 Electrical Characteristics of the Discharge

Voltage and current are monitored continuously and displayed in real time on the digital oscilloscope, which is also interfaced to a computer and data files are stored on the computer. The instantaneous power was calculated from the voltage and current waveforms for all experiments at different flow regimes and different gas (He and O_2) mixing ratios at atmospheric pressure. The complex impedance of the discharge, as explained in Chapter 2, was used to obtain plasma parameters from the solution of the plasma dielectric constant. As the discharge is initiated by a sinusoidal voltage at low frequency, then the voltage across the discharge is also sinusoidal although not smooth due to the series of breakdowns taking place in the plasma.. The current and the voltage have the V-I phase difference at the same frequency, which is not perfectly 90° in a cylindrical capacitive plasma discharge system. The plasma circuit model provides a solution to the phase angle via the difference between the voltage and the current. To find the V-I phase difference; the power factor is defined as the ratio between the average power and the apparent power. The average power is obtained by averaging the product of the voltage and current waveforms, obtained from oscilloscope data, and tabulated versus the time. In other words, the dissipated power in the plasma equals the average power over one period. The dissipated power in watts (W) is defined as

$P_{ave} = \frac{1}{\tau} \int_0^\tau V_{LF}(t) I_{LF}(t) dt$, and the apparent power in Volt-Amps (VA) is defined as

$P_{apparent} = I_{RMS} \times V_{RMS}$ in which $V_{RMS} = \sqrt{\dfrac{1}{\tau}\int_0^\tau V_{LF}^2(t)dt}$ and $I_{RMS} = \sqrt{\dfrac{1}{\tau}\int_0^\tau I_{LF}^2(t)dt}$. Thus, the

ratio between the average and apparent powers in the plasma is denoted as the power

factor $\cos\phi$. Power factor measurements are carried out to calculate the V-I phase difference,

and RMS voltage and current values are measured from the voltage and current waveforms.

Figure 8 shows the voltage and current waveforms of the coaxial discharge with pure helium

at a flow rate of 10,000sccm as the working gas, and in absence of substrate.
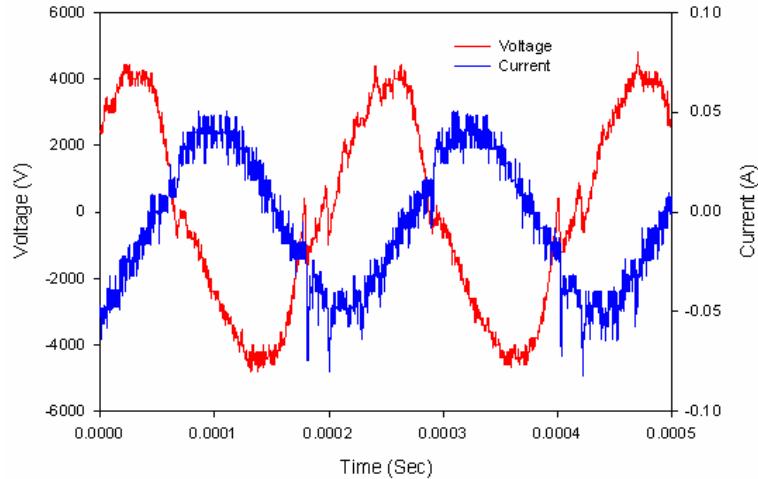
Figure 9 Voltage and Current waveforms of pure helium discharge at 10,000sccm flow rate in absence of substrate

As seen from Fig. 9 the voltage and current signals are nearly out of phase,

waveforms are distorted and indicate the presence of streamers and micro arcs. The RMS

values are obtained from the measured waveforms while taking into account any distortions.

The power factor can be considered as a displacement power factor because of the distortion,

and the phase angle determines the phase difference of voltage and current.

Figure 10 shows the phase difference with and without a sample in the plasma. As seen from the figure, there is no significant difference in the phase for the current waveforms due to the fact that the current is more displacement over conduction. There is slight difference in the voltage, however, it is not conclusive as a major phase change. The phase difference between the voltage and current in both cases is approximately identical, thus indicating no significant effect from the yarn on the plasma formation or its dielectric constant.
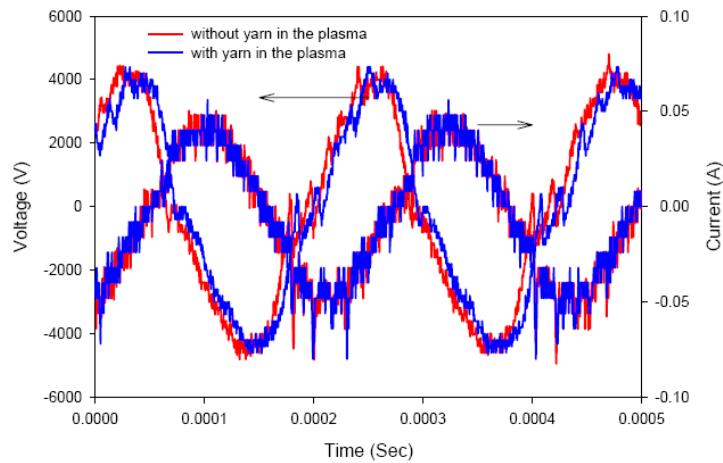
Figure 10 Voltage and current waveforms with and without yarn in the plasma for a pure helium discharge at 10,000sccm mass flow rate

Figure 11 shows the change in the voltage waveform as the oxygen flow rate is increased from 23sccm to 100sccm in 10,000sccm helium discharge. The voltage amplitude increases with increased oxygen flow rate and shifts in time. It is also observed that the pure helium discharge has streamers and arcing as seen from the breakdowns and jumps in the waveform. With increased flow of oxygen the waveform becomes smoother. The peak-to-peak voltage for the pure helium discharge is ~8kV and that for the 100sccm oxygen in the helium is ~16kV, a factor of 2 higher; and the voltage peak shift is about 40-50µsec.
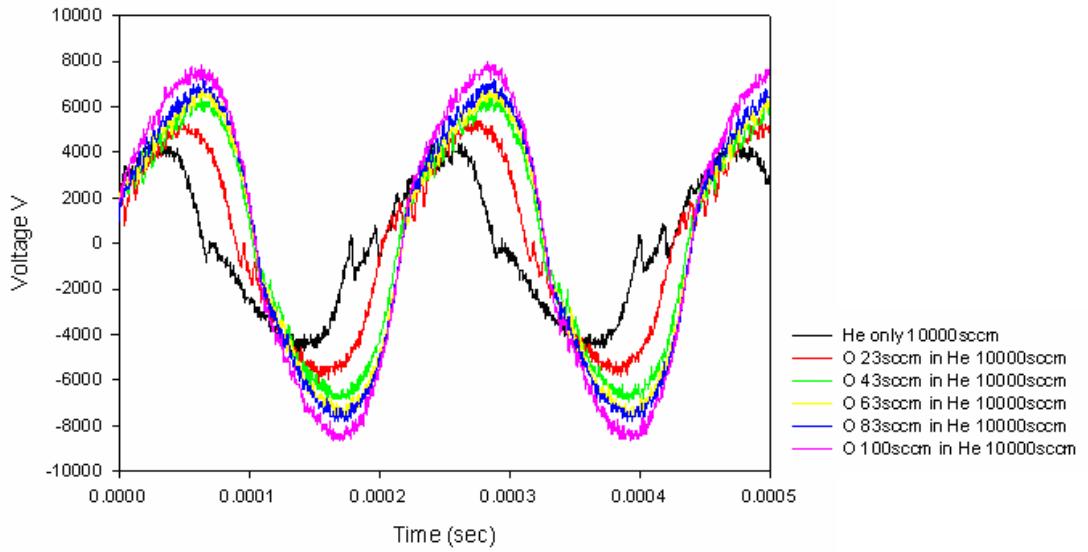
Figure 11 Voltage waveform for various oxygen flow rates in the helium discharge in absence of substrate (no yarn in the discharge)

Figure 12 shows the increase in the voltage (peak-to-peak) with increased oxygen flow rate. It is clear that the increase in the voltage is linear with increased oxygen flow rate following the linear fit equation $V_{pp(kV)} = 8.23 + 0.076 \ \dot{m}_{(sccm)}$ with $R^2 = 0.98476$, where $V_{pp(kV)}$ is the peak-to-peak voltage and $\dot{m}_{(sccm)}$ is the oxygen mass flow rate.
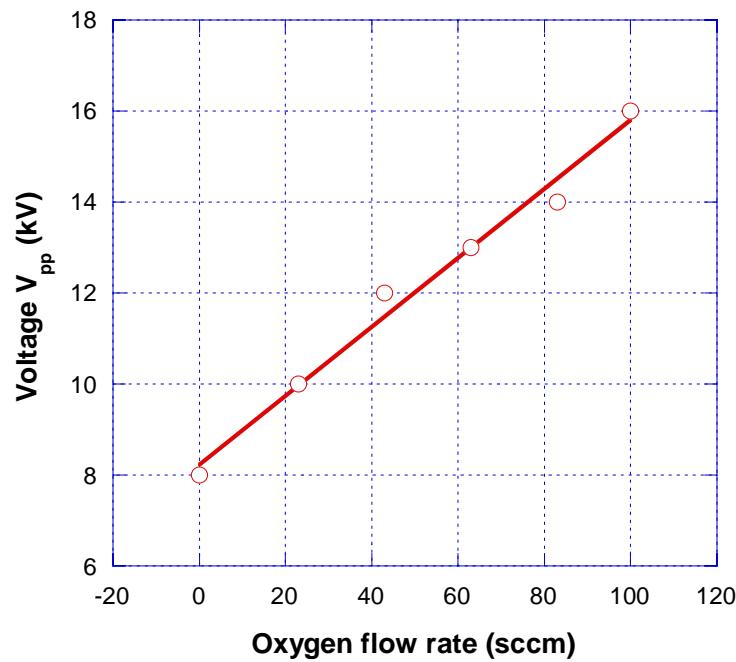
Figure 12 Peak-to-peak voltages versus oxygen mass flow rate in absence of substrate

Figure 13 shows the phase shift in the current waveform, about 40-50μsec lagging for oxygenated helium plasmas as compared to pure helium one. The shift is identical for all oxygen flow rates indicating no effect from increased oxygen flow rate on the current phase shift. Streamers are evidential in the discharge for pure helium, as seen from the spikes in the waveform, as well as the oxygenated helium waveforms, however, less streamers with oxygen flowing in the discharge.
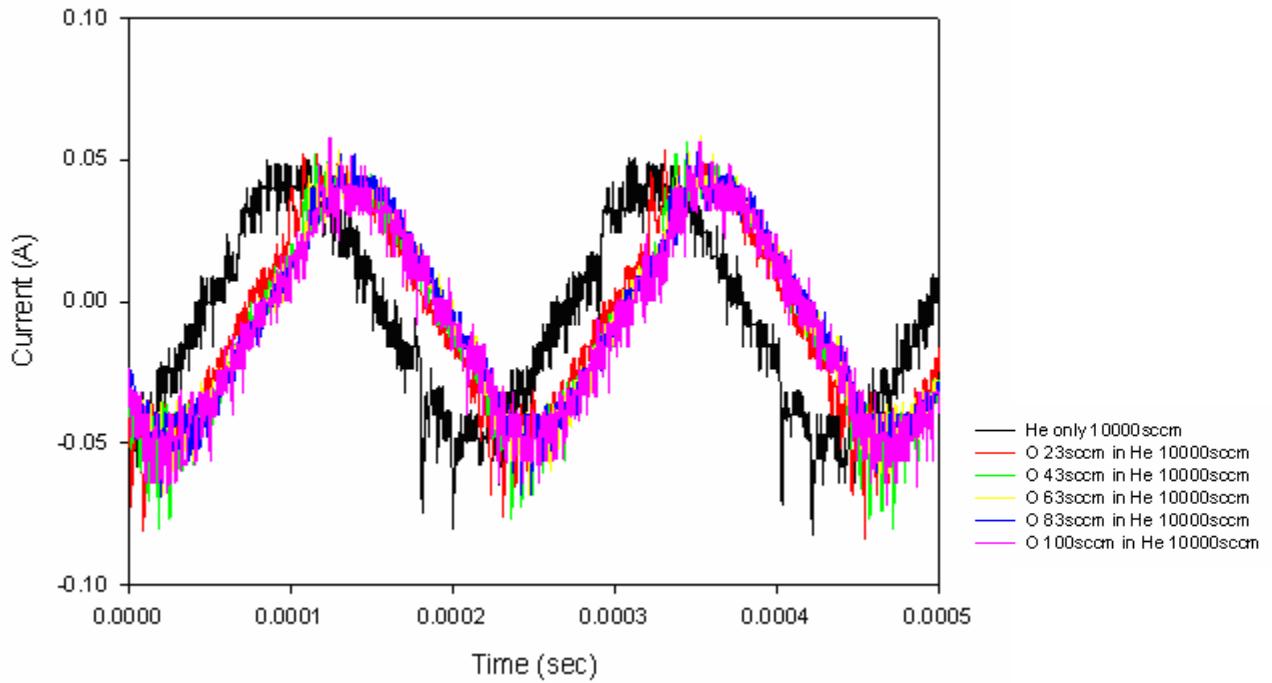
Figure 13 Current waveform for various oxygen flow rates in the helium discharge in absence of substrate (no yarn in the discharge)

Figure 14 shows the change in the voltage waveform with the increase in oxygen flow rate from 23 to 100sccm in 10,000sccm helium discharge. The voltage amplitude increases with increased oxygen flow rate and shifts in time, as previously observed in the experiment without substrate. Again, the pure helium discharge has streamers and arcing as seen from the breakdowns and jumps in the waveform, however, once oxygen is introduced into the discharge the waveform becomes smoother. The peak-to-peak voltage for the pure helium discharge is ~8kV and that for the 100sccm oxygen in the helium is ~17kV, still about a factor of 2 but slightly higher than that without yarn in the discharge; and the voltage peak shift is about 45-55μsec, slightly higher than that without yarn in the discharge.
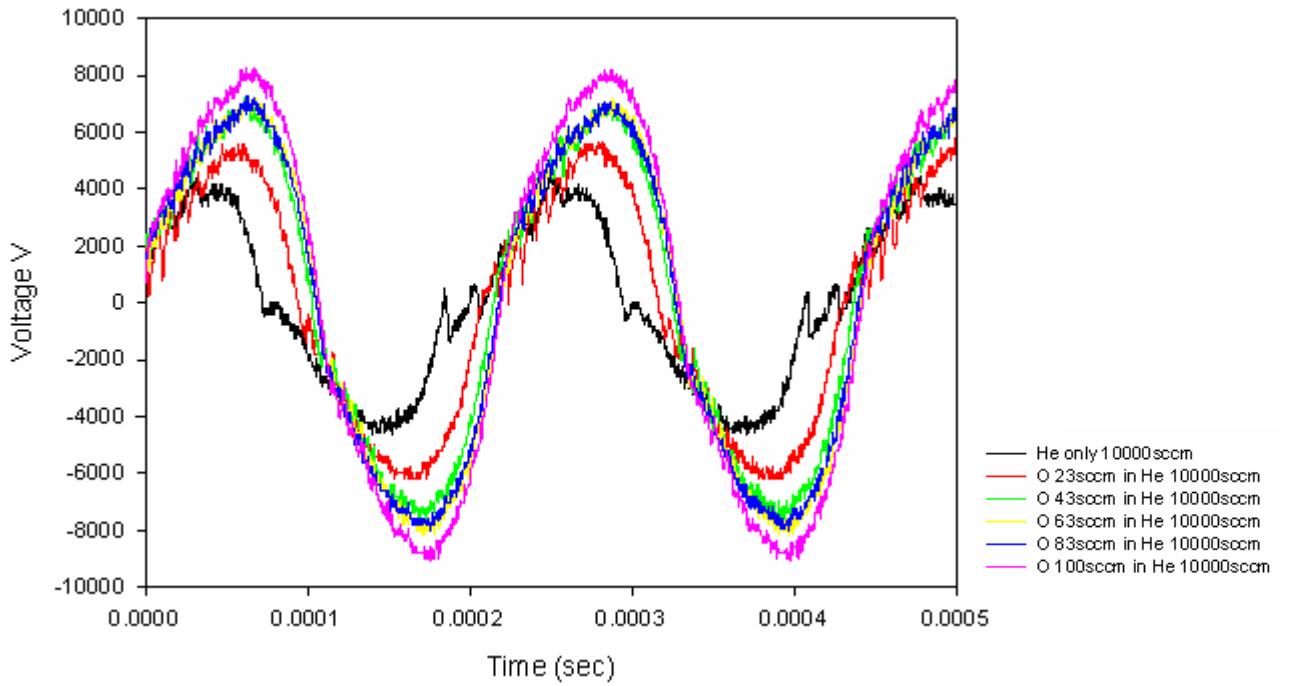
Figure 14 Voltage waveform various oxygen flow rates in the helium discharge in presence of substrate (a yarn is immersed in the discharge)

Figure 15 shows the increase in the voltage (peak-to-peak) with increased oxygen flow rate in presence of a substrate (yarn) in the discharge. The increase in the voltage is linear with increased oxygen flow rate following the linear fit equation $V_{pp(kV)} = 8.98 + 0.08 \; \dot{m}_{(sccm)}$ with $R^2 = 0.90128$, where $V_{pp(kV)}$ is the peak-to-peak voltage and $\dot{m}_{(sccm)}$ is the oxygen mass flow rate. As seen from the graph, there is a slight change in the magnitude of the peak-to-peak voltages as well as a change in the linearity, indicating the effect of the yarn as to slightly increase the voltage with increased oxygen content. This also is associated with the oxygen etching effect on the yarn that changes the effective dielectric

constant of the entire discharge and consequently the discharge equivalent electric admittance.
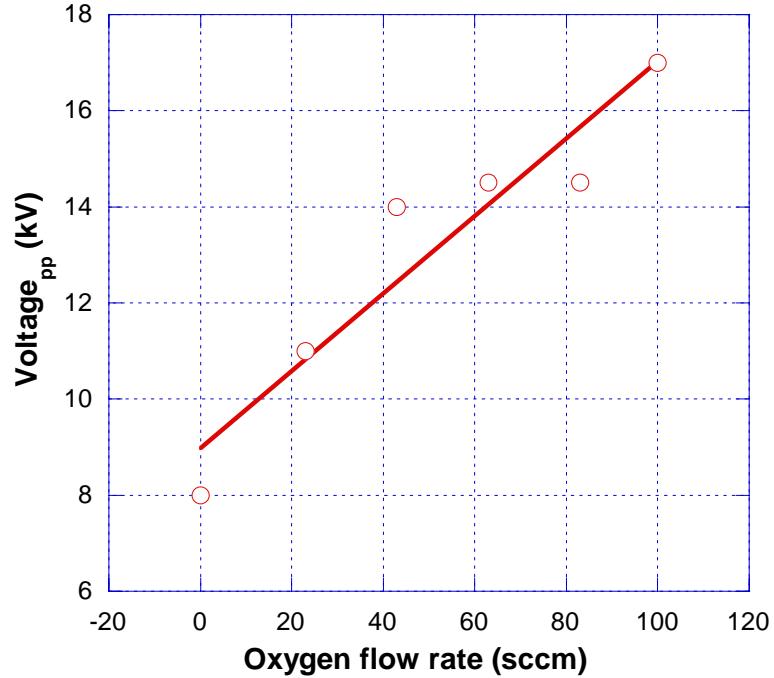
Figure 15 Peak-to-peak voltage versus oxygen mass flow rate in presence of substrate

A comparison of the change in the peak-to-peak voltage in absence and presence of yarn in the discharge is shown in Figure 16 in which the change in the peak-to-peak voltage is higher for 43 and 63sccm oxygen flow rates, as well as at higher rates. This suggests that the etching of the yarn at 43 and 63sccm takes place then a mixed etching/re-combination follows at higher flow rates. Once radicals' population increases, as well as additional ionized species, then the plasma dielectric constant changes, which results in affecting the plasma admittance and hence the peak-to-peak voltage.
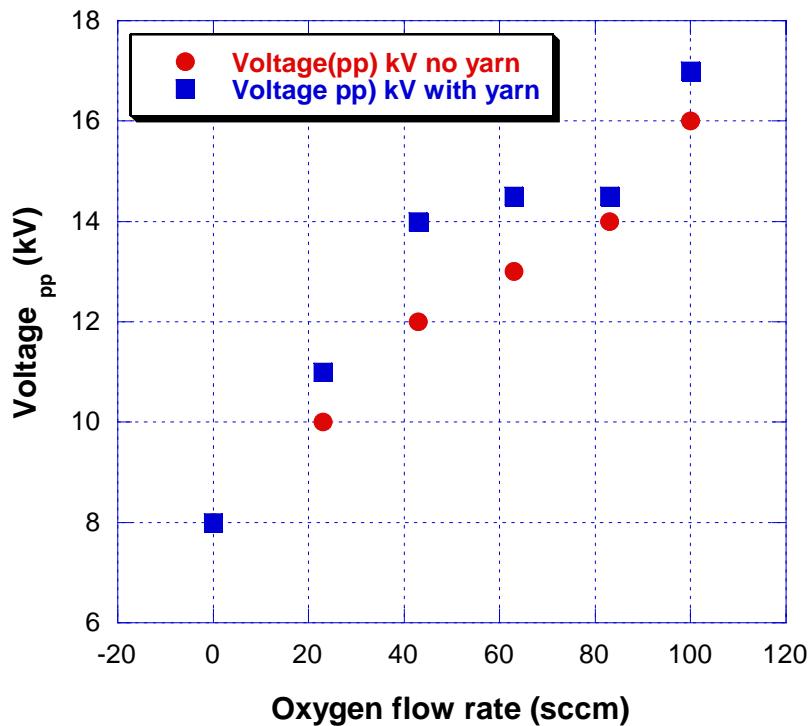
Figure 16 Comparison of the peak-to-peak voltage versus oxygen mass flow rate in absence and presence of yarn in the discharge

Figure 17 shows the phase shift in the current waveform in presence of a yarn in the plasma, about 40-50μsec lagging for oxygenated helium plasmas as compared to pure helium one, which is similar to that obtained for the discharge in absence of yarn. Again, the shift is near identical for all oxygen flow rates indicating no effect from increased oxygen flow rate on the current phase shift. Pure helium discharge experience more streamers, however, less streamers with oxygen flowing in the discharge.
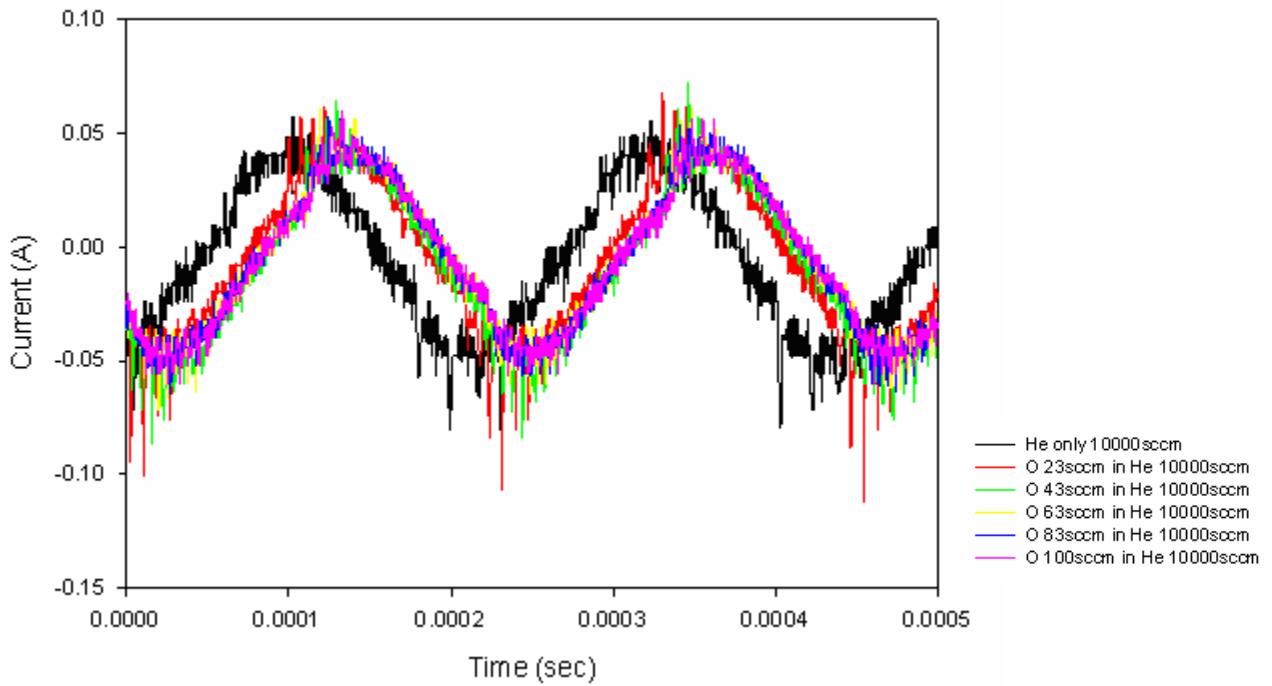
**Figure 17 Current waveform for various oxygen flow rates in the helium discharge in presence of substrate (yarn is immersed in the discharge)**

Electrical properties are examined based on the circuit analysis, voltage and current waveforms, phase shifts and change in peak-to-peak voltage with and without substrate in the plasma, as shown in the set of Figures 14, 15, 16 and 17. One can recognize that the discharge is not absolutely symmetric in terms of the positive and negative half cycles, as seen from the voltage and current waveforms because the discharge is characterized with a self-bias voltage drop across the electrodes. The RMS voltage and current are calculated from the waveforms to allow for the calculation of the apparent power delivered into the plasma. Figures 18 and 19 compare the peak-to-peak and RMS values for the discharge voltage and current, respectively.

36

As shown in Fig. 18, the peak-to-peak and RMS voltage values increase when a sample (cotton yarn) is immersed in the plasma. This increase is about 1kV peak-to-peak (~0.5kV RMS) for the oxygen flow range between 23 and 63sccm after which there is no voltage increases with increased oxygen flow rate beyond 83sccm. The increase in the voltage is attributed to the change in the plasma dielectric constant due to addition of etched materials from the surface of the yarn; however, saturation is reached at 83sccm oxygen flow rate and no more etching would take place.
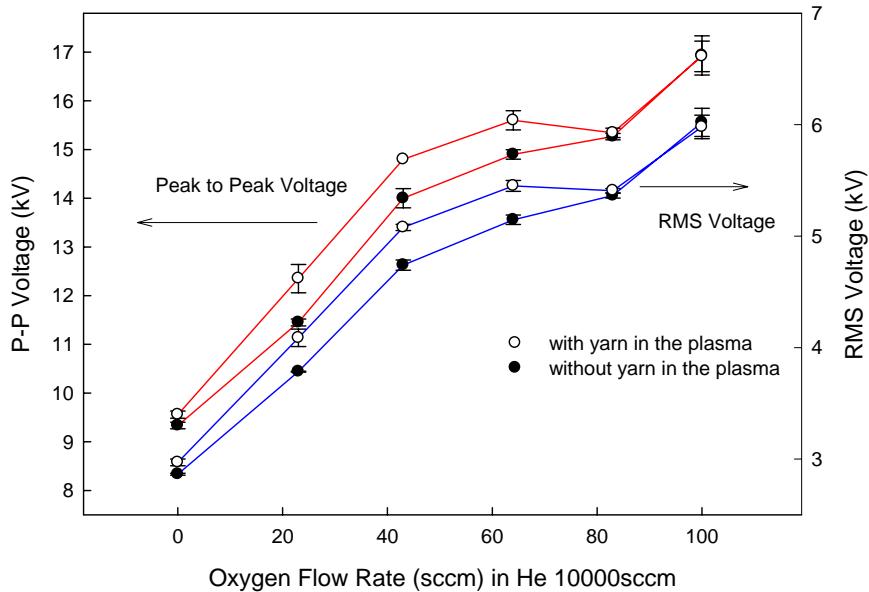
Figure 18 Peak to Peak and RMS voltages of the discharge, in absence and presence of a substrate (cotton yarn), as a function of the oxygen mass flow rate in a constant 10,000sccm helium flow

Figure 19 shows the peak-to-peak and RMS current values, which indicates a general trend of decreased current with increased oxygen flow into the helium plasma. This decrease in the current with increased oxygen content is indicative of the change in the plasma impedance as the power into the plasma, from the power supply, is constant at each pre-determined gas flow rate. The observed initial increase in the peak-to-peak current at 23sccm oxygen may be attributed to a sudden etching of the yarn surface that sharply changed the

plasma admittance, at increased flow rates there is no appreciable change in the current when the yarn is immersed in the plasma. Likewise, the RMS current has slight increase with the yarn in the plasma at lower flow rates of 23 and 43sccm then the magnitudes resume to same level with and without the yarn in the plasma. The RMS current drops from ~185mA for pure helium discharge to ~31mA when 100sccm oxygen is added to the gas flow.
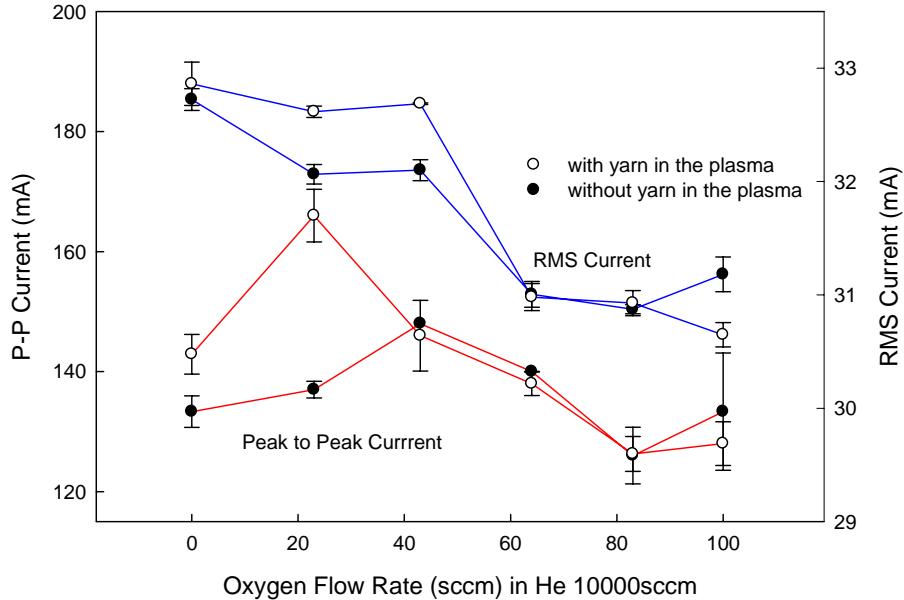
Figure 19 Peak to Peak and RMS currents of the discharge, in absence and presence of a substrate (cotton yarn), as a function of the oxygen mass flow rate in a constant 10,000sccm helium flow

The plasma model described in Chapter 3 related electrical parameters, voltage and current, to the equivalent impedance from which the solution for the plasma dielectric constant yields equations for the electron number density and the collision frequency. Figure 19 shows the impedance, and the admittance (reciprocal of the impedance), in absence and presence of a substrate (cotton yarn), as a function of the oxygen mass flow rate in a constant 10,000sccm helium flow. The impedance increases with increased oxygen flow in the

discharge. The impedance is the absolute value of its complex form and is calculated from the RMS values of voltage and current. As previously shown, the voltage increases with increased oxygen flow rate but the current decreases and hence it is clear that the rate of voltage increase is higher than the rate of current decrease resulting in increased impedance. This also indicates the change in the plasma dielectric constant following the change in the oxygen/helium mixing ratio. There is a slight increase in the impedance when the yarn is immersed in the plasma at oxygen flow rate between 23 and 63sccm, which may be attributed to an etching effect and release of etched molecules from the yarn into the plasma, however, saturation takes place at 83sccm oxygen flow and the impedance is similar with and without yarn in the plasma. The equation for admittance, in complex variable form as derived in Chapter 3, shows high dependence on the plasma electron number density, indicating decrease in admittance when electron number density decreases.

$$Y = \frac{\dfrac{C_0 e^2 n_e}{m_e \varepsilon_o \nu_m}}{\left(\dfrac{C_0 e^2 n_e}{m_e \varepsilon_o \nu_m}\right)^2 + \left(-\dfrac{C_0 e^2 n_e}{m_e \varepsilon_o \omega} + C_0\omega\right)^2} + j\left(C_D\omega + \frac{\dfrac{C_0 e^2 n_e}{m_e \varepsilon_o \nu_m} - C_0\omega}{\left(\dfrac{C_0 e^2 n_e}{m_e \varepsilon_o \nu_m}\right)^2 + \left(-\dfrac{C_0 e^2 n_e}{m_e \varepsilon_o \omega} + C_0\omega\right)^2}\right)$$

One may expect an increase in the number density with addition of more oxygen in the discharge, but as the total energy input per each gas mixing ratio is held constant and the plasma temperature would remain almost unchanged then recombination with incoming oxygen takes place, As a result of recombination, the number density decreases and consequently the admittance decreases (impedance increases with addition of neutral oxygen).
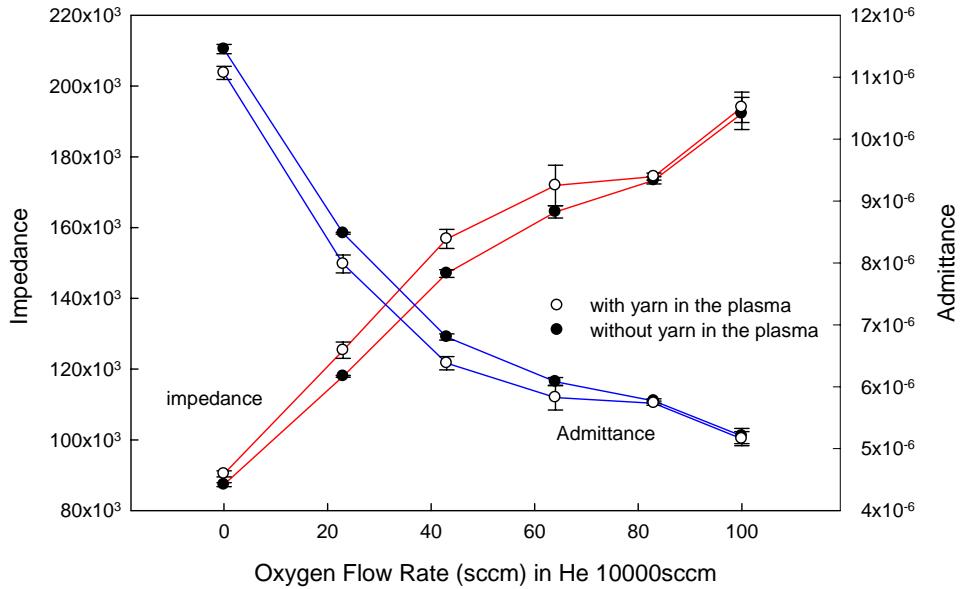
Figure 20 Impedance and admittance, in absence and presence of a substrate (cotton yarn), as a function of the oxygen mass flow rate in a constant 10,000sccm helium flow

The average dissipated power (in Watts), is the average power over one discharge period $P_{ave} = \frac{1}{\tau} \int_0^\tau V_{LF}(t) I_{LF}(t) dt$, it is the true power dissipated in the plasma.

The apparent power (measured in Volt-Amp) is the combination of dissipated power and the reactive power $P_{apparent} = I_{RMS} \times V_{RMS} = \left(\frac{1}{\tau} \int_0^\tau V_{LF}^2(t) dt \right)^{\frac{1}{2}} \left(\frac{1}{\tau} \int_0^\tau I_{LF}^2(t) dt \right)^{\frac{1}{2}}$; it is the sum of the power in the resistive and reactive components. The phase difference is derived by the power factor that represents the portion of the apparent power. Figure 20 shows the average and apparent power as a function of the oxygen mass flow in absence and presence of the substrate. The average "dissipated" power increases by 80 Watts and the apparent power increases by 100 Watts as the oxygen flow is increased from zero to 100sccm. There is a

slight increase in both powers when a substrate is immersed in the plasma, however, at high

oxygen flow rates there is no appreciable difference.
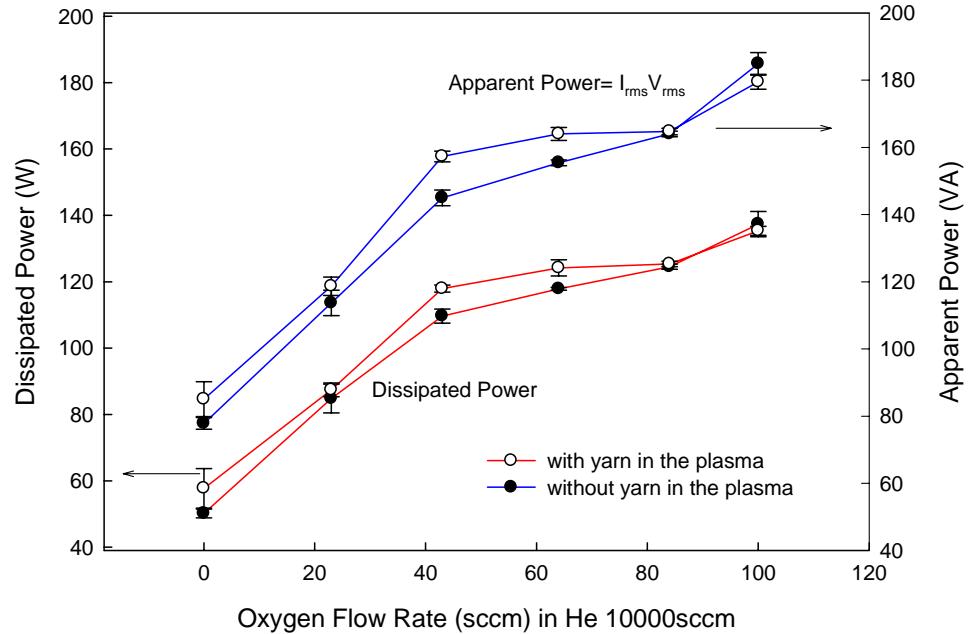
Figure 21 Average and apparent power, in absence and presence of a substrate (cotton yarn), as a function of the oxygen mass flow rate in a constant 10,000sccm helium flow

Essentially, this dissipated power is in the form of Joule (Ohmic) heating

$P = \frac{1}{2}|E|^2 \sigma \frac{v^2}{\omega^2 + v^2} A$, where E is the electric field intensity, σ is the plas ma conductivity,

v is the electron-neutral collision frequency, ω is the frequency with the electric field

oscillates and A is the discharge cross sectional area. The increase in the dissipated energy

with increased oxygen content is due to the increased electrical resitivity of the plasma,

which means reduction in the conductivity in the above equation. Because of the fact that the

discharge frequency is in the kHz range, which is much less than the electron-neutral

collision frequency, then the Joule dissipation is approximated to $P \cong \frac{1}{2}|E|^2 \sigma A$ indicating

the plasma is close to a pseudo steady state DC glow discharge. The change in the V-I phase

difference is shown in Figure 21 as a function of the increase in the oxygen content. The

phase difference decreases with increased oxygen flow rate, which is in correlation with the

above mentioned analysis of increased resistivity. As plasma becomes more resistive, the

phase difference between the current and voltage becomes smaller and when plasma is fully

resistive the phase difference approaches zero. In the current setup the plasma is not fully

resistive, the maximum phase angle is 57° for pure helium discharge and drops to 42° when

the oxygen flow increases to100sccm in the plasma. There is no appreciable change in the

phase angle with a yarn immersed in the plasma indicating no, or minimal, effect on the

plasma resistivity.
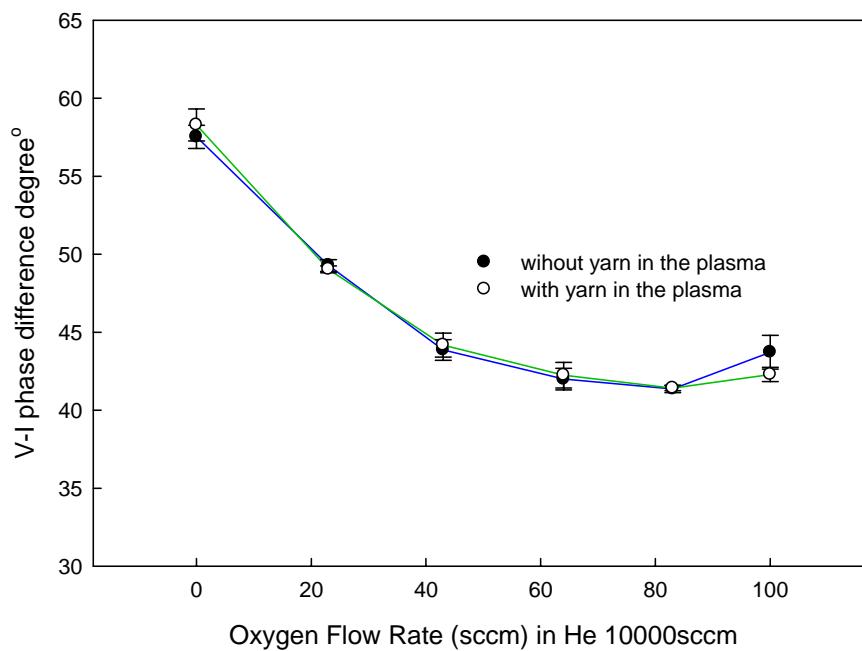
Figure 22 V-I phase difference, in absence and presence of a substrate (cotton yarn), as a function of the oxygen mass flow rate in a constant 10,000sccm helium flow

4.2 Plasma electron number density and electron-neutral collision frequency

As previously shown in Chapter 3, the plasma model for the admittance is given by

$$Y = \frac{\dfrac{C_0 e^2 n_e}{m_e \varepsilon_o v_m}}{\left(\dfrac{C_0 e^2 n_e}{m_e \varepsilon_o v_m}\right)^2 + \left(-\dfrac{C_0 e^2 n_e}{m_e \varepsilon_o \omega} + C_0 \omega\right)^2} + j\left(C_D \omega + \frac{\dfrac{C_0 e^2 n_e}{m_e \varepsilon_o v_m} - C_0 \omega}{\left(\dfrac{C_0 e^2 n_e}{m_e \varepsilon_o v_m}\right)^2 + \left(-\dfrac{C_0 e^2 n_e}{m_e \varepsilon_o \omega} + C_0 \omega\right)^2}\right)$$

From decoupling the equation of admittance, the electron number density and the electron-neutral collision frequency are given by the following equations

$$n_e = \frac{m_e \varepsilon_o \omega v_m}{e^2} \frac{C_D C_0 \omega^2 - 1 - A C_0 \omega \sin\delta}{C_D C_0 v_m \omega - A C_0 (\omega\cos\delta + v_m \sin\delta)}$$

$$v_m = \omega\left(1 - 2 C_D C_0 \omega^2\right)\tan\delta + \frac{\omega^2 \left\{A^2 C_0 + C_D (C_D C_0 \omega^2 - 1)\right\}}{A \cos\delta}$$

As seen from the equations, the electron-neutral collision frequency can be obtained from the knowledge of the phase angle and other discharge geometry parameters. Upon obtaining the electron-neutral collision frequency a substitution into the electron number density equation provides solution to obtain the number density. These two equations can also be solved in real time to obtain the time behavior of the collision frequency and the electron number density. Figure 23 shows the change in the electron-neutral collision frequency as a function of the change in the oxygen flow rate in the helium plasma, in absence and presence of cotton yarn in the plasma. The electron-neutral collision frequency increases from 70 kHz for pure helium discharge to 125 kHz when 100sccm oxygen is introduced into the plasma. The increase in the collision frequency is due to increased number of heavy molecules, oxygen, into the discharge which changes the plasma resistance

$R_p = v_m L_p$ where $L_p = 1/\omega_{pe}^2 C_o$ and hence $R_p = \dfrac{v_m}{\omega_{pe}^2 C_o} = \dfrac{v_m m_e \varepsilon_o}{n_e e^2 C_o}$. Expressing the collision frequency in terms of the plasma resistance shows that an increase in the collision frequency is expected when the resistance increases $v_m = R_p \dfrac{n_e e^2 C_o}{m_e \varepsilon_o}$. Slight increase in the collision frequency was observed when the yarn was exposed to the plasma for the oxygen flow rate between 23 and 63 sccm which may be attributed to additional change in the plasma total resistance; however, there is no observable change in the collision frequency for higher oxygen flow rates.
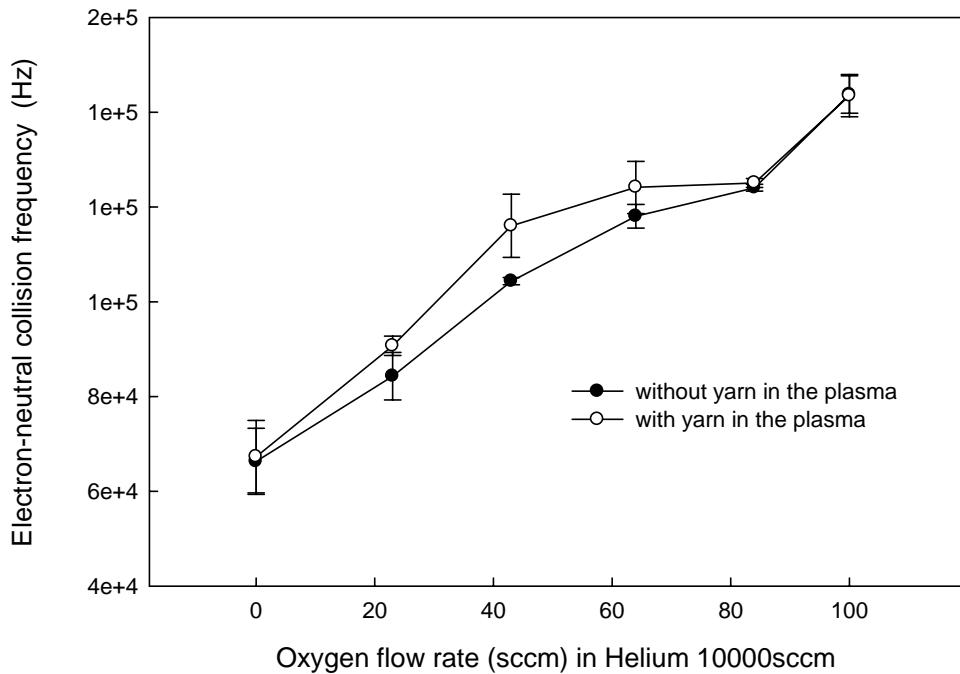
Figure 23 Electron–neutral collision frequency, in absence and presence of a substrate (cotton yarn), as a function of the oxygen mass flow rate in a constant 10,000sccm helium flow

The electron-neutral collision frequency was used in the electron number density equation to obtain the plasma electron density over the range of increased oxygen flow rate. Figure 24 shows the electron number density, in absence and presence of a substrate (cotton

yarn), as a function of the oxygen mass flow rate in a constant 10,000sccm helium flow. In

pure helium discharge, the electron number density is ~2.1 x 10^{16}/m^3, and decreases as

oxygen is introduced into the discharge. As oxygen is added at 23sccm, the electron number

density drops to1.75 x 10^{16}/m^3, and continues to decrease with increased oxygen flow rate

1.6 x 10^{16}/m^3, and levels off for higher flow rates up to 100sccm. The decreases in electron

number density indicates increased recombination rate coefficient when oxygen is added to

the helium plasma. Although etching of substrate (cotton yarn) may take place during

exposure to oxygenated plasma, however the substrate has no effect on the electron number

density and no observed change as seen from Figure 23.
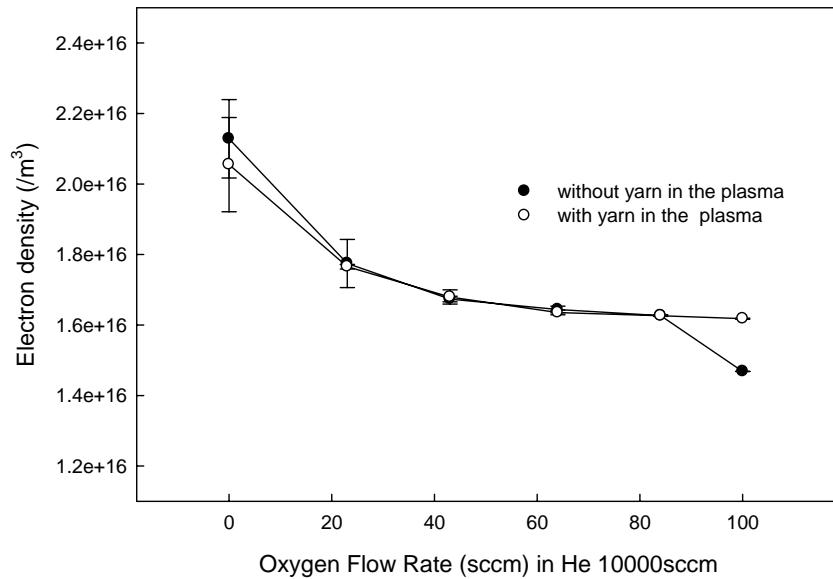
Figure 24 Electron number density, in absence and presence of a substrate (cotton yarn), as a function of the oxygen mass flow rate in a constant 10,000sccm helium flow

It is important to look into the change in the electron-neutral collision frequency

(Figure 24) and the correlation to the change in the electron number density (Figure 23),

45

these changes show that as the more neutral gas molecules (oxygen) are introduced in to the plasma the collision frequency increases, which indicates high collisional effects in the discharge. Increased collisional effects is due to electrons' impact on oxygen ions and other species (resulting from surface etching of the yarn), and hence the electron number density decreases. The increase in the electron–neutral collision frequency is also due to the fact that the thermal conductivity of oxygen is higher than that of helium [33]. From measurement of the current and voltage it has been shown that the impedance increases indicating an increase in the plasma resistivity η, which is directly proportional to the collision frequency and inversely proportional to the electron number density $\eta = \dfrac{m_e \nu_m}{e^2 n_e}$. Figure 24 shows the calculated plasma resistivity, in absence and presence of a substrate (cotton yarn), as a function of the oxygen mass flow rate in a constant 10,000sccm helium flow. It is clear that the plasma resistivity increases with increased oxygen content in the helium discharge. The electron-neutral collision frequency increases due to the increased effect of electron-oxygen collision. The effect of the collision frequency is dominant in the resistivity equation and hence the shape of the resistivity graph resembles that of the electron-neutral collision frequency graph. Again, there is no appreciable change in the plasma resistivity when the yarn is immersed in the plasma, indicating a minimal effect on the entire discharge behavior, i.e. no major change in the discharge impedance.
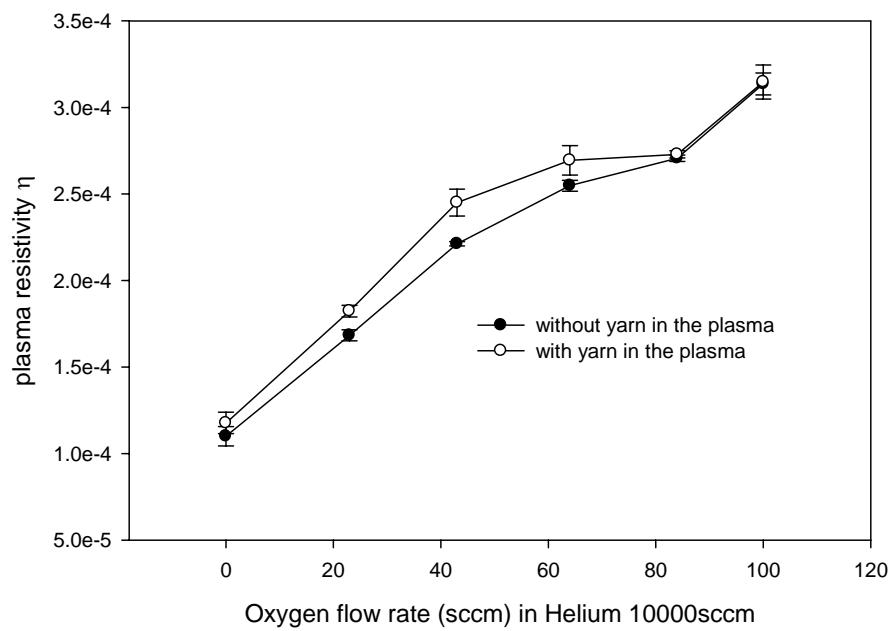
Figure 25 Calculated plasma resistivity, in absence and presence of a substrate (cotton yarn), as a function of the oxygen mass flow rate in a constant 10,000sccm helium flow

4.3 Optical Emission Spectroscopy Results and Analysis

Optical emission spectra were taken for the various gas mixtures in absence and presence of yarn in the plasma. Optical emission spectroscopy was performed with Ocean Optics HR2000CG-UV-NIR spectrometers, with spectral resolution of 1 nm and over a spectral range 450 - 750 nm. Figure 25 shows the emission lines of the discharge without yarn in the plasma. For pure helium discharge, atomic helium lines 471.314nm, 492.193 nm, 501.567 nm, 587.562 nm, 706.519 nm, and 728.135 nm are identified. The intensity of the 705.51nm lines is quite high and this intensity drops dramatically when oxygen is introduced into the discharge, and continues to decrease as the oxygen content increases. However, oxygen lines were not observed and probably their intensity is very low as the discharge is dominated by helium with a flow rate of 10,000sccm. It is also possible that fractional ionization of oxygen is very low as compared to helium.
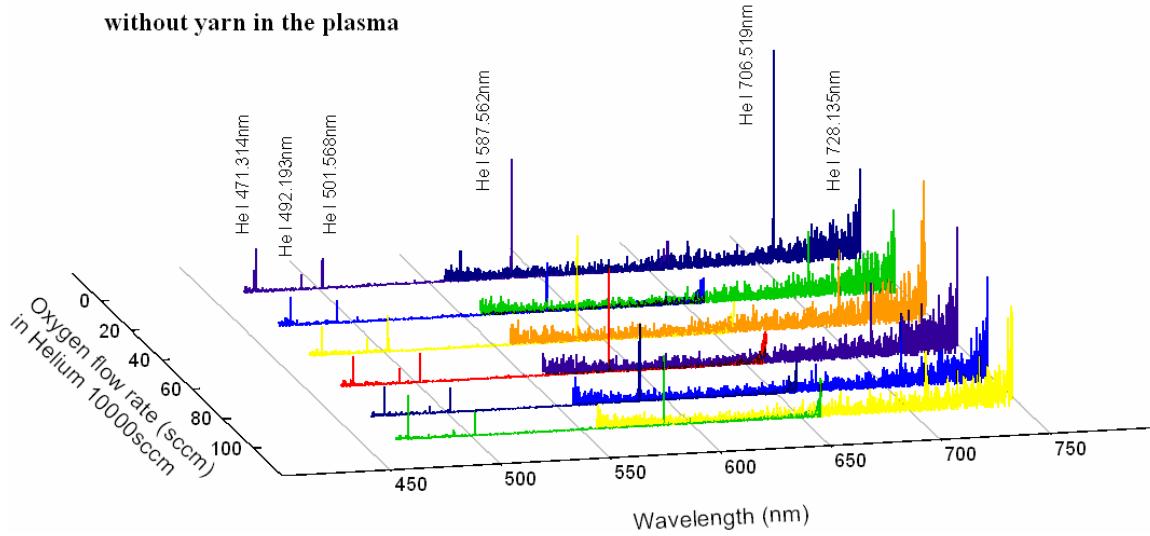
Figure 26 Optical emission spectra (OES) of the helium–oxygen DBD plasma in absence of substrate as a function of the oxygen mass flow rate in a constant 10,000sccm helium flow

Figure 26 shows the spectra with cotton yarn in the plasma. The only observed difference from the spectra without yarn in the plasma is that the helium 587.562 nm line is more intense and remains with almost same intensity even with oxygen addition to the discharge. The intensity of the 705.51nm drops with increased oxygen content in the plasma, which is similar to the case of no substrate in the plasma.
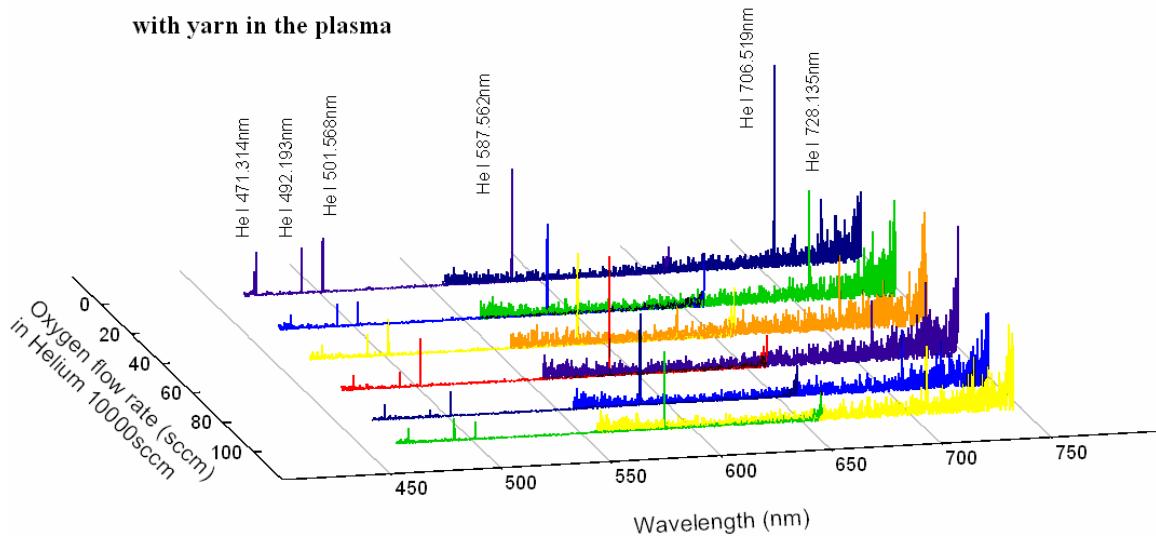
**Figure 27 Optical emission spectra (OES) of the helium–oxygen DBD plasma, in presence of a cotton yarn exposed to plasma, as a function of the oxygen mass flow rate in a constant 10,000sccm helium flow**

Plasma electron temperature was calculated using the Boltzmann plot of He I lines assuming plasma is at LTE. Table 2 shows spectral data of helium I lines, which were used to obtain the electron plasma temperature.

Table 2Helium I spectral data [33]

Element	Wavelength (nm)	A_{ki} (10^8 s^{-1})	g_k	E_k (eV)	Transition			
	471.315	5.89E-02	3	23.5939573	$1s2p$ $^3P°$	—	$1s4s$	^3S
	492.193	2.02E-01	5	23.7363336	$1s2p$ $^1P°$	—	$1s4d$	^1D
He I	501.568	1.34E-01	3	23.0870172	$1s2s$ ^1S	—	$1s3p$	$^1P°$
	587.562	2.94E-01	3	23.0736551	$1s2p$ $^3P°$	—	$1s3d$	^3D
	706.519	1.54E-01	3	22.7184651	$1s2p$ $^3P°$	—	$1s3s$	^3S
	728.135	1.81E-01	1	22.9203161	$1s2p$ $^1P°$	—	$1s3s$	^1S

An example of Boltzmann plot is shown in Fig. 27 for the case of oxygen flow at 43sccm in 10,000sccm helium without yarn in the plasma. These data were obtained from helium lines 471.314nm, 492.193 nm, 501.567 nm, 587.562 nm, 706.519 nm, and 728.135 nm. Figure 28 shows the Boltzmann plot for the same helium lines when a yarn is immersed in the plasma. As seen from Figure 28 the electron temperature with the yarn in the plasma increases from 0.26eV to 0.35eV while the electron density decreases as shown from the solution of the electrical model.
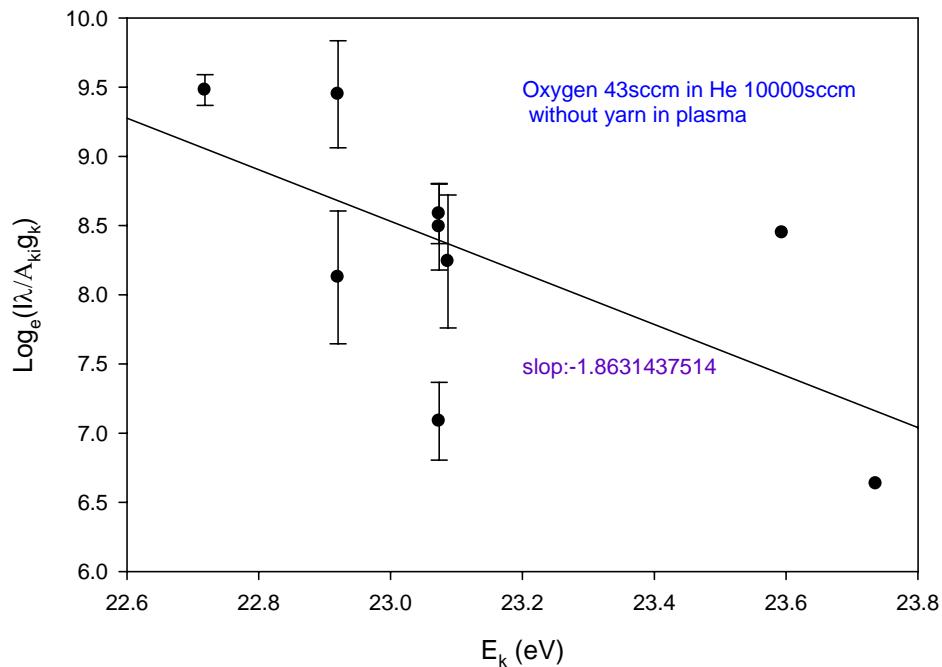
Figure 28 Boltzmann plot using helium lines for the case of oxygen 43sccm in 10,000 sccm helium without a yarn in the plasma
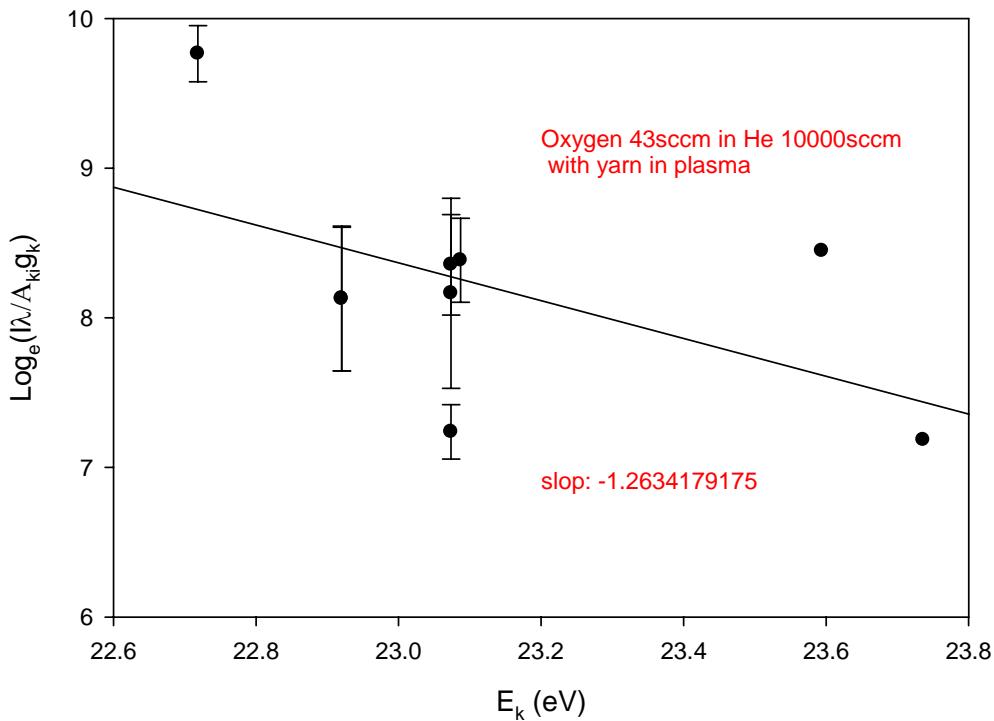
Figure 29 Boltzmann plot using helium lines for the case of oxygen 43sccm in 10,000 sccm helium with a yarn in the plasma

The plasma temperature as a function of the oxygen flow rate in the helium discharge, in absence and presence of yarn in the plasma, is plotted in Fig. 30 in which the temperature varies between 0.2 to 0.35eV. The electron plasma temperature is slightly higher when a yarn is immersed in the plasma, however, within experimental errors and limitations of the optical emission spectroscopy certainties it is safe to state that the plasma temperature in absence of yarn is about 0.25eV, and about 0.3eV in presence of yarn. In fact, these results do not differ and the variations seen in Figure 30 are not indicative of a true change in the plasma temperature. The most conservative estimate, based on these results, is that the plasma temperate is between 0.2 -0.3eV in this discharge.
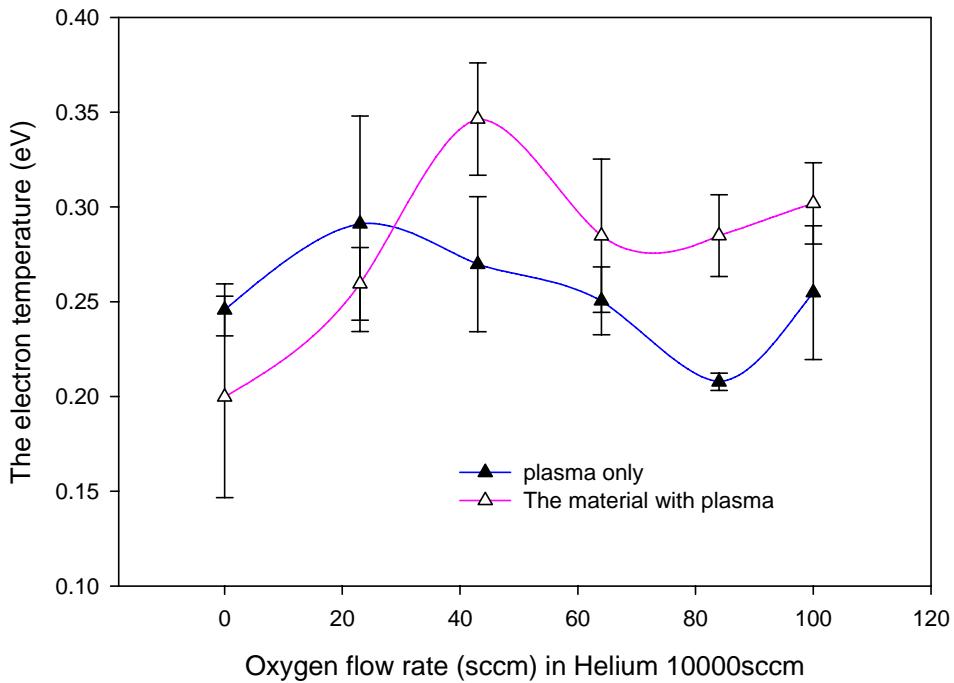
Figure 30 Electron plasma temperature as a function of oxygen flow rate in absence and presence of yarn in the plasma

Because the discharge has streamers, it is expected that the electron temperature of the streamers is much higher than that of the discharge. Figure 30 shows the streamers' electron temperature as calculated from a Boltzmann plot using lines of He I (471.314nm, 706.519 nm, and 728.135 nm). The results indicate that the streamers electron temperature in presence of yarns is less that that without yarns. Also observed is that the streamers' electron temperature increases with increased oxygen flow rate. The temperature without yarn in the plasma averages to about 1.0eVwhile it averages to about 0.6eV in presence of yarns. The increase in the temperature with increased oxygen content approaches 1.5eV in both cases. It appears that plasma in this configuration produces more of a streamer corona discharge over the DBD glow discharge.
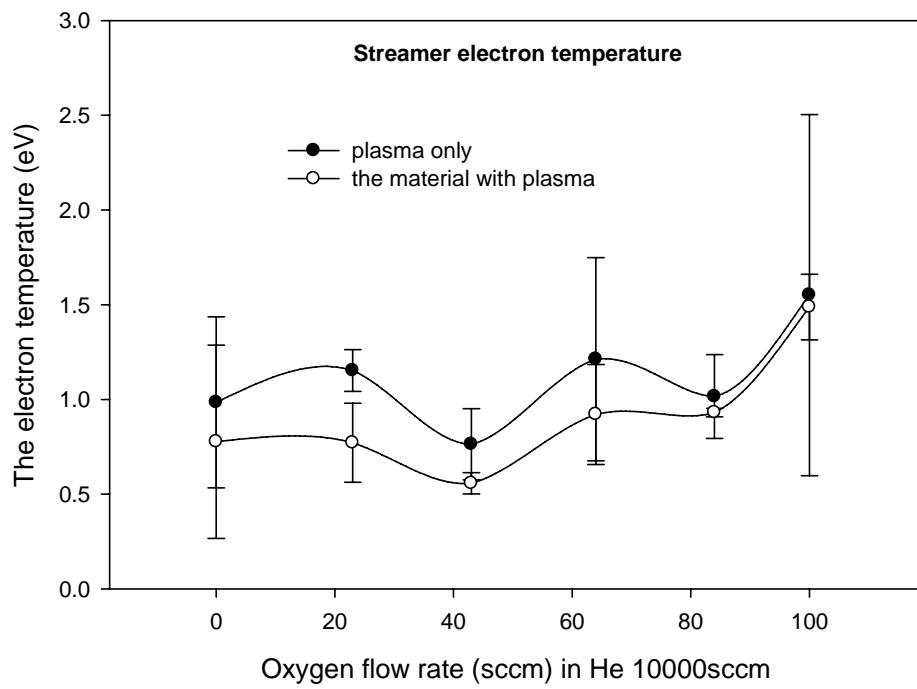
Figure 31 Electron temperatures of plasma streamers obtained from helium data (471.314nm, 706.519 nm, and 728.135 nm helium lines)

4.4 Substrate Surface Analysis

Analysis of the surface of exposed yarn was conducted using a Hitachi variable pressure S-3200 Scanning Electron Microscope (SEM) to obtain magnified pictures of exposed samples, as well as the surface elemental analysis via Energy Dispersive X-ray Spectroscopy (EDS).

Figure 32 shows an example of EDS for a cotton yarn indicating the elemental composition of the surface, where the elemental composition is determined by the peaks of each detected element. This sample is for the case of oxygen flowing at 43sccm in 10,000sccm helium (a case that shows the highest electron plasma temperature).
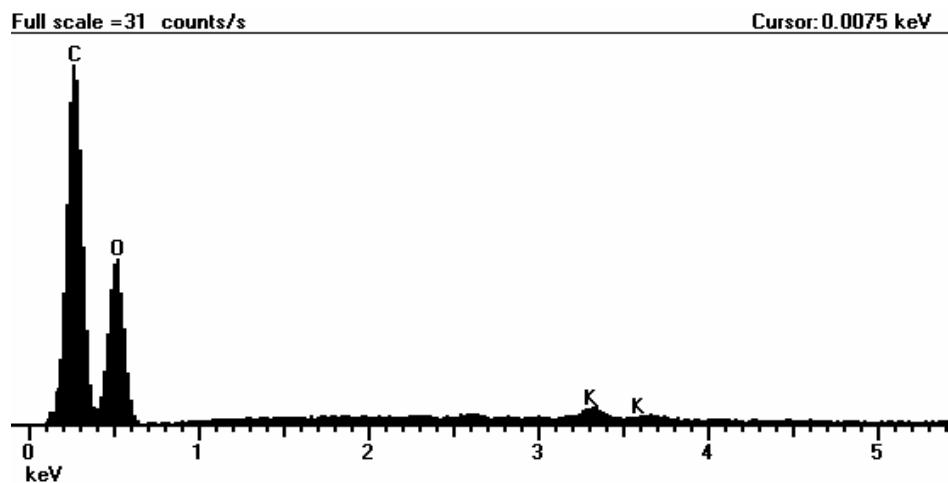
Figure 32 EDS spectra of elements detected in yarn sample exposed to oxygenated helium plasma (Oxygen 43sccm/He 10,000sccm), showing higher carbon to oxygen abundance

As seen from the Figure 32 the surface is, principally, composed of carbon and oxygen. Normalized oxygen to carbon ratio can be obtained from the oxygen and carbon abundance components from each EDS's amplitude for each sample. Average values of the balance components may be used to obtain more accurate O/C ratio when the components are

from a mix of the yarn samples under various plasma conditions. Figure 31 shows the normalized O/C ratio as a function of the oxygen mass flow rate in 10,000 sccm helium plasma. Raw yarn has a normalized O/C ratio of 0.48 and the ratio slightly increases to 0.49 when exposed to pure helium plasma. In fact, there is no change in the O/C ratio when the yarn sample was exposed to pure helium plasma as there is no further oxygen content in the discharge. Additionally, there is no surface etching or polymer chain scission to allow for adding oxygen from the yarn's broken bonds. As oxygen flow rate was increased to 23sccm, the O/C ratio dropped to 0.45, which may be attributed to release of carbon from broken bonds. This trend continues when the oxygen flow rate was increased to 43sccm, the O/C ratio dropped to 0.33. Further increase in oxygen flow rate resulted in an increase in the O/C ratio from that of the 43sccm case. This means that the increased oxygen flow rate may caused increased partial diffusion of oxygen into the surface and the O/C ratio recovers back to 0.45 at 83sccm oxygen and exceeds the raw sample ratio when oxygen flow rate was increased to 100sccm (O/C ~ 0.53). It is also possible that increased oxygen flow rate beyond 43sccm promotes surface etching and scission, which releases oxygen from the substrate's surface, thus increasing the O/C ratio.

The EDS data indicates dependence of plasma ashing on the oxygen flow rate. The plasma ashing rate has a minimum point at 43sccm oxygen and the entire graph has a V-shape as a function of the oxygen flow rate. The oxygen induces plasma ashing and removes the carbon from the sample's surface due to the high chemical reaction rates of oxygen radicals with the substrate surface.
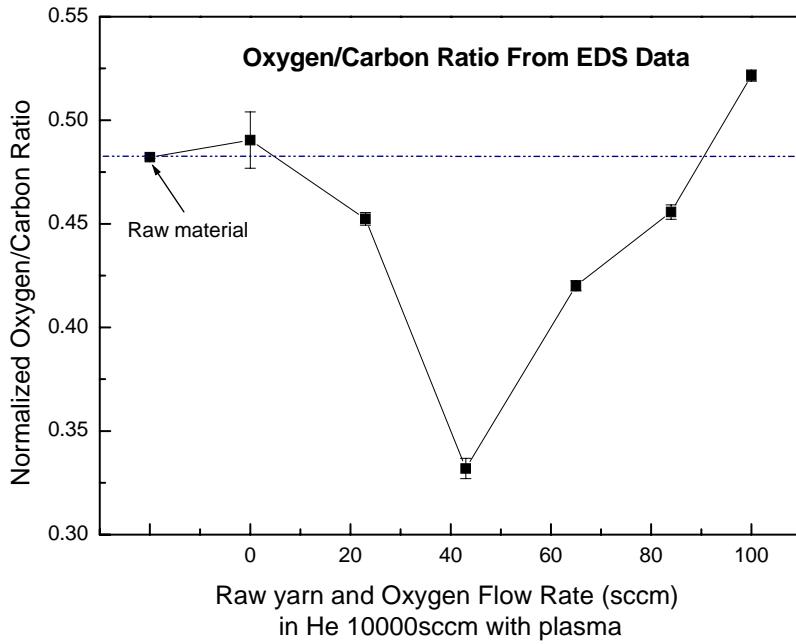
Figure 33 Normalized O/C ratio from EDS spectra as a function of the oxygen mass flow rate in the helium plasma

SEM micrographs of the yarn show surface smoothness after exposure to oxygenated helium plasma, probably due to surface etching and possible oxidation. Figure 34 is a SEM micrograph of the raw yarn sample, while Figures 35 and 36 are for samples exposed for 5 minutes to helium plasmas with 43sccm and 100sccm oxygen, respectively. Correlating SEM pictures and surface morphology to the O/C ratio analysis indicates that the gas mixture has an effect on the composition on the surface. As O/C ratio shows increased ratio with increased oxygen content beyond the minimum value at 43sccm oxygen, it is apparent that the plasma processing has high affinity for oxygen, which in turn would affect the electrical properties of the entire discharge when a yarn is immersed in the plasma due to increased oxygen abundance.
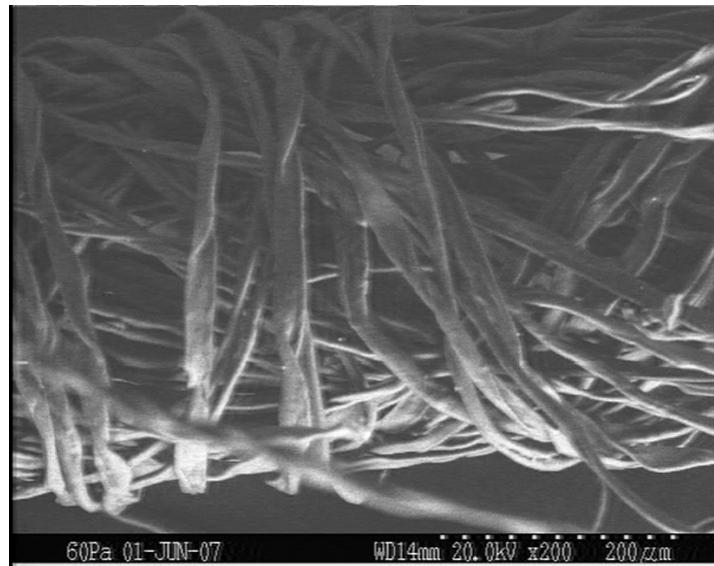
Figure 34 SEM micrograph of raw yarn not exposed to plasma
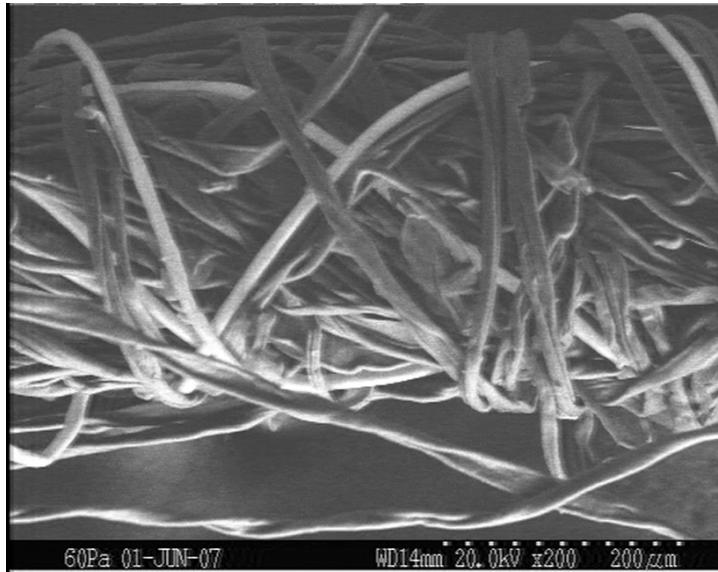
Figure 35 SEM micrograph of a the yarn exposed to plasma with 43sccm oxygen in 10,000sccm helium for 5 minutes
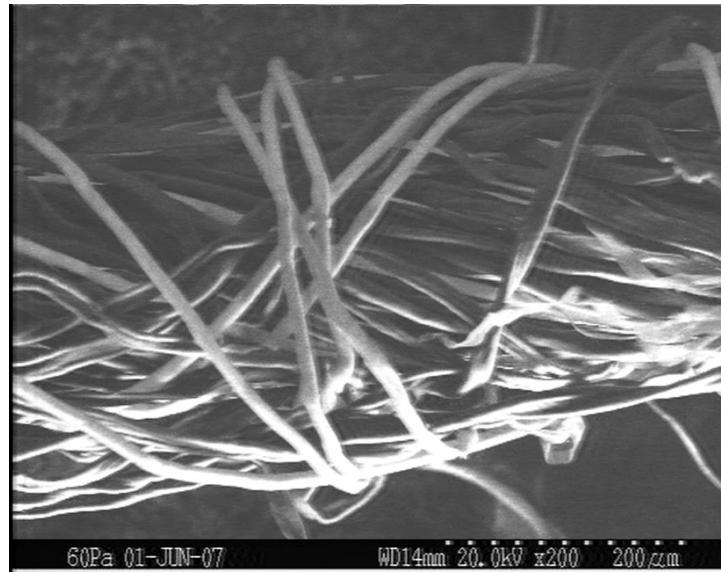
Figure 36 SEM micrograph of a the yarn exposed to plasma with 100sccm oxygen in 10,000sccm helium for 5 minutes

Since oxygen can significantly change the plasma processing, the plasma parameters obtained by solving the plasma impedance can be influenced by the oxygen reactions in the discharge and interaction of oxygen radicals with the surface of the substrate, thus controlling oxygen flow rate can determine the optimum operating conditions. As seen from Figures 34, 35 and 36, the white filament surfaces may be correlated to growth of oxygen and its partial diffusion into the surface during plasma processing. The increase of the oxygen flow rate promotes the activity and reaction with the filaments. Oxygen diffusion/deposition is clearly increased when the oxygen flow rate was increase to 100sccm, as seen from Figure 32.

Chapter 5

Discharge Thermal Behavior

5.1 Electron Temperature from the Discharge I-V characteristics

An estimate of the electron plasma temperature can be obtained from investigating the discharge current-voltage relation using a simplified model based on the power balance. The time-averaged power absorbed can be written as

$$P_{abs} = \underbrace{\frac{1}{\tau}\int_0^\tau I_{LF}(t) \cdot V_{LF}(t)dt}_{Mesuremant} = \frac{1}{\tau}\int_0^\tau \vec{J}_{LF}(t) \cdot \vec{E}_{LF}(t)\mathcal{V}_{eff}\,dt$$

where $\mathcal{V}_{eff}$ is the effective volume of the plasma and $I_{LF}(t)$ and $V_{LF}(t)$ are the current and voltage of the low-frequency discharge, respectively. The current and voltage are measured (Pearson coil for current and high voltage probe for voltage). The time-averaged absorbed power P_{abs} by electrons and ions can be calculated using the following equation.

$$P_{abs} = P_{ohm} + 2P_{rand} + P_{ion}$$

where P_{ohm} is the ohmic heating of electrons, P_{rand} is the electron randon heating in the oscillating sheathes of the discharge and P_{ion} is the power transferred to ion.

Upon substitution for the power terms in the above equation, the equation can be re-written as

$$P_{abs} = \frac{1}{2}\frac{m}{e^2 n}\frac{I_{LF}^2}{A_{eff}^2}A_{eff}\left(\nu_m d_{eff} + 2\bar{v}_e + 3u_B \frac{\omega_{pe}^2}{\omega^2}\right)$$

where $\bar{v}_e = \sqrt{\dfrac{8eT_e}{\pi m}}$ is the mean electron speed, $u_B = \sqrt{\dfrac{eT_e}{M}}$ is the Bohm velocity for ions,

$\omega_{pe}^2 = \dfrac{e^2 n}{\varepsilon_0 m}$ is the electron plasma frequency, $\mathcal{V}_{eff} = A_{eff} d_{eff}$ is the effective volume, ν_m is the

electron-neutral collision frequency, T_e is the electron temperature in unit of volts, M is ion

mass, m is electron mass and n is the electron number density. A_{eff} and d_{eff} are the discharge

effective cross sectional area $A_{eff} = 2\pi\left(R_2^2 - R_1^2\right) + 2\pi h\left(R_2 + R_1\right)$ and the effective diameter

$d_{eff} = \dfrac{\pi\left(R_2^2 - R_1^2\right)h}{A_{eff}}$, respectively.

Solving for the electron plasma temperature:

$$eT_e = \left(\frac{\dfrac{P_{abs} A_{eff}}{I_{LF}^2} - \dfrac{m\nu_m d_{eff}}{2e^2 n}}{\left(\dfrac{m}{e^2 n}\sqrt{\dfrac{8}{\pi m}} + \dfrac{3}{2\varepsilon_0 \omega^2}\sqrt{\dfrac{1}{M}}\right)}\right)^2$$

The plasma temperature, obtained from solution of the above equation, as a function of the

oxygen flow rate in the helium discharge, in absence and presence of yarn in the plasma, is

plotted in Fig. 37 in which the temperature varies between 0.4 to 2.2eV. These temperatures

are much higher that temperatures obtained from optical emission spectroscopy (OES).

However, temperatures of streamers obtained from OSE are in the range $0.6 - 1.5$eV. The

model does not distinguish between streamers temperatures and electron temperatures and

thus the temperature obtained from the model represents an estimate of the time-averaged

electron plasma temperature assuming all power is absorbed in electron and ion heating

mechanisms. As seen from Figure 37, the temperature increases with the increase in oxygen

content in the discharge, indicating the effect of increased collisional processes that increase

ohmic heating. There is no appreciable difference when a yarn is immersed in the plasma, indicating negligible effect from particles etched from the surface on plasma electron temperature, in other word the etched particulates does not produce appreciable change in the electron-neutral collisions.
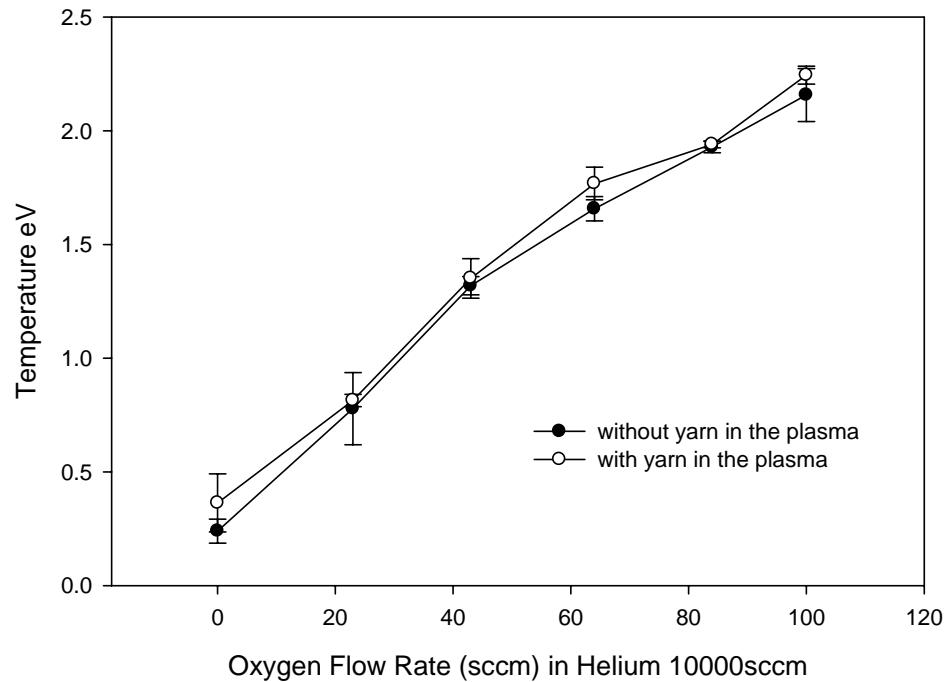
Figure 37 Electron plasma temperature, calculated from the power balance model, as a function of oxygen flow rate in absence and presence of yarn in the plasma

5.2 Plasma Losses

Internal Power Losses

The plasma internal thermal losses are calculated with and without yarn in the plasma at different oxygen flow rates in 10,000sccm helium flow. Electron number density obtained from discharge electrical measurements and plasma dielectric model solution, and electron plasma temperature obtained from optical emission spectroscopy result were used to

calculate the internal energy losses. Internal power loss is calculated from

$$P_E = \frac{3}{2}\frac{kT_e}{\tau}\left(n_{electron} + n_{ion}\right)\mathcal{V}_{eff}\,watt$$, where τ is the discharge duration and $\mathcal{V}_{eff}$ is the

discharge effective volume [34,35]. The internal power loss as a function of the oxygen flow rate in the helium discharge, in absence and presence of yarn in the plasma, is plotted in Figure 38, in which the loss is about 0.1 watt in the pure helium discharge and increases to about 0.6 watts at 100sccm oxygen flow into the discharge. As seen from the Figure 38 the internal power loss increases as a consequence of increased resistivity due to the increase in collisional energy transfer as more oxygen is introduced into the discharge. The electrical power transferred to electrons is mostly used for maintaining the plasma state by ionization and excitation, and the amount of internal power loss is minimal.
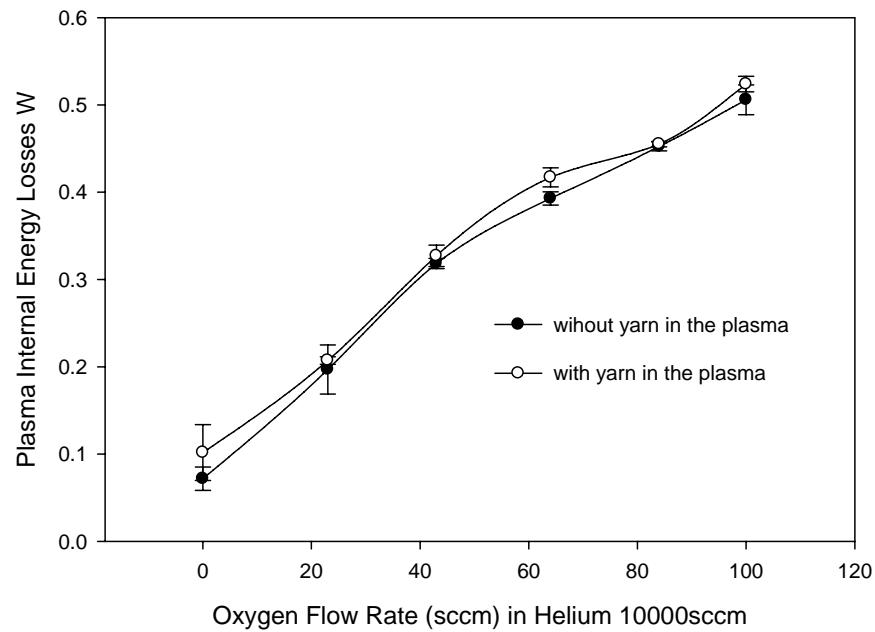

Figure 38 Internal Power Loss as a function of oxygen flow rate in absence and presence of yarn in the plasma

Plasma Radiation Losses

The energy lost from the plasma due to deceleration mechanisms are mostly in the form of bremsstrahlung radiation, and that due to electron transitions will result in atomic line radiation.

The Bremsstrahlung power radiated from the plasma is given by

$$P_{BR} = 1.69 \times 10^{-32} \underset{cm^{-3}}{\underbrace{n_e}} \underset{eV}{\underbrace{T_e^{1/2}}} \sum n_Z Z^2 \mathcal{V}_{eff} \ watt$$

where Z is the ionization state of the n_z species in the plasma [34,35]. Figure 39 shows Bremsstrahlung power loss as a function of oxygen flow rate in absence and presence of yarn in the plasma. It is clear that the bremsstrahlung power loss is negligible and does not affect the discharge power balance.
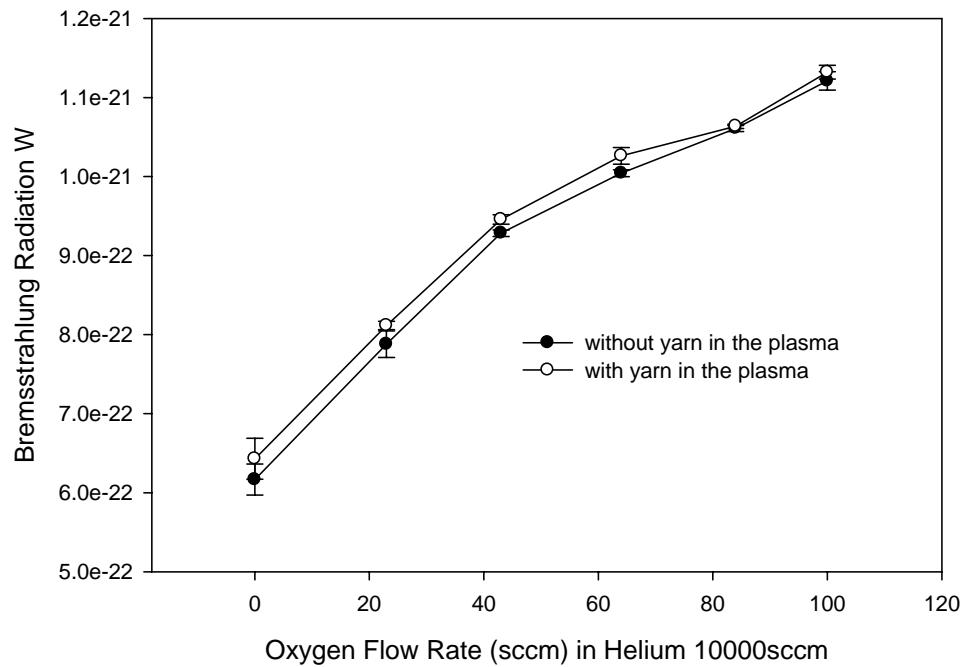

Figure 39 Bremsstrahlung power loss as a function of oxygen flow rate in absence and presence of yarn in the plasma

The atomic line power radiated from the plasma is given by [35]

$$P_{LR} = 8 \times 10^{-23} \underbrace{n_e n_Z}_{cm^{-3}} Z^6 \underbrace{T_e^{-3/2}}_{keV} \mathcal{V}_{eff} \ watt$$

Figure 40 shows atomic line radiated power as a function of oxygen flow rate in absence and presence of yarn in the plasma. The power loss is about 1.0 mW when no oxygen is introduced into the discharge, and drops to almost zero as oxygen contents are increased, thus indicating negligible atomic line radiation losses.
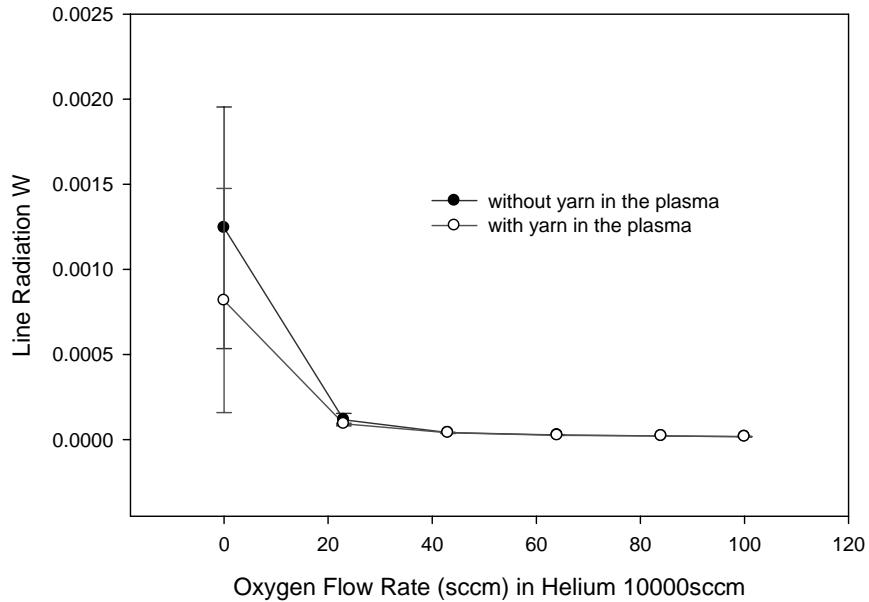
Figure 40 Line Radiation Power Loss as a function of oxygen flow rate in absence and presence of yarn in the plasma

5.3 Total Discharge Power Balance

The total power balance in the discharge indicates that most of the power is absorbed in the plasma in Joule heating. The losses due to internal power loss, Bremsstrahlung and atomic line radiation are negligible. Figure 41 shows the dissipated power, internal power loss and atomic line radiated power (Bremstrahlung is neglected). It is clear that the power

into the discharge is mostly dissipated in electron, and ion, heating mechanisms and that the

losses due to radiation and internal power losses are negligible. The total dissipated power is

in the range of 100 watts, consistent with the results previously shown in Figure 21 (Chapter

3), where it was shown that the dissipated power varies between 60 -120 watts.
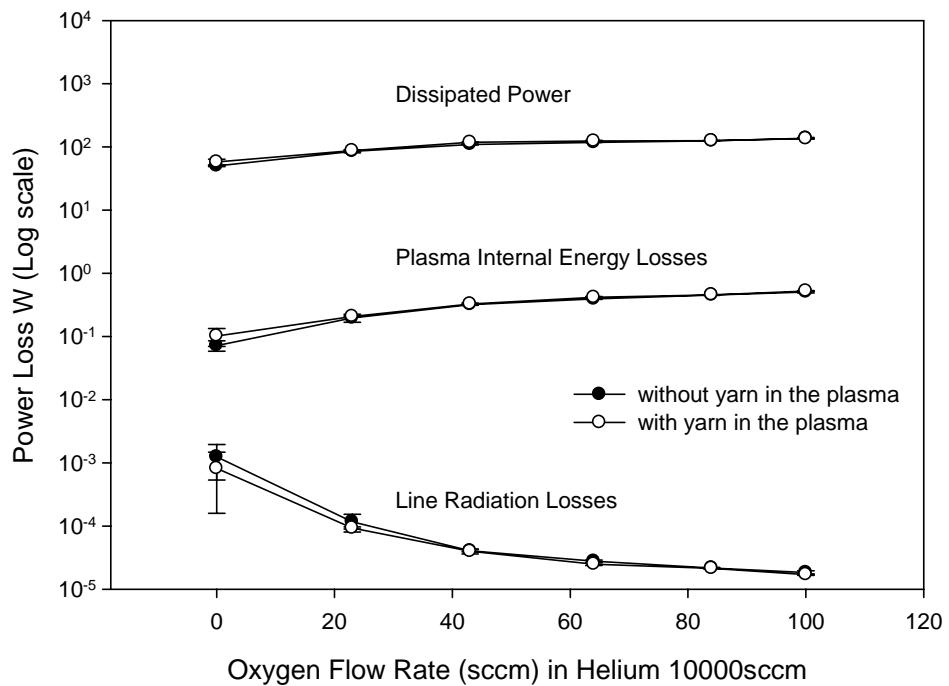
**Figure 41 Comparison between total dissipated power and power Losses as a function of oxygen flow rate in absence and presence of yarn in the plasma**

Chapter 6

Conclusion

Plasma characteristics in a cylindrical coaxial capacitively-coupled, low-frequency (LF) atmospheric pressure Dielectric-Barrier Discharge (DBD) were investigated over a wide range of oxygen mixing ratio into helium. Experiments were conducted in absence and presence of cotton yarns to determine the effect of the discharge on yarn treatment. The fundamental characteristics of plasma parameters were investigated. A model based on measured electrical paramteres was developed and used to calculate the electron number density and the electro-neutral collision frequency. Another simplified model for discharge power balance was used to evaluate the electron plasma temperature and compare the results to values obtained from optical emission spectroscopy. The electron-neutral collision frequency increases with increased oxygen contents in the discharge while the electron number density decreases due to increase recombination rates. The electron number density varies between 1.6- 2.1 x 10^{16}/m^3 over the entire range of change of oxygen content. Optical emission spectroscopy has shown electron temperature in the range of 0.2 -0.3eV, while the range for the temperature of the streamers was found to be 0.6-1.5eV. The power balance model has shown higher temperatures in the range of 0.4 to 2.2eV.

Power balance and discharge thermal behavior revealed that the power input to the discharge is mostly dissipated in heating electrons and ions and that the losses are minimal, thus indicating good discharge efficiency.

Energy Dispersive X-ray Spectroscopy (EDS) was used to obtain the O/C ratio of the treated cotton yarn samples. There was no change in the O/C ratio when the yarn sample was exposed to pure helium plasma. As oxygen flow rate was increased the O/C ratio increased to 0.49 but dropped with further increase in oxygen content, however, further increase in oxygen flow rate resulted in an increase in the O/C ratio to recover back to to 0.45 at 83sccm oxygen and exceeds the raw sample ratio when oxygen flow rate was increased to 100sccm (O/C ~ 0.53). The EDS data indicates dependence of plasma ashing on the oxygen flow rate. The plasma ashing rate has a minimum point at 43sccm oxygen and the entire graph has a V-shape as a function of the oxygen flow rate. The oxygen induces plasma ashing and removes the carbon from the sample's surface due to the high chemical reaction rates of oxygen radicals with the substrate surface.

The SEM micrographs of the exposed yarns show surface smoothness, which are attributed to surface etching and possible oxidation. Correlating SEM pictures and surface morphology to the O/C ratio analysis indicates that the gas mixture has an effect on the composition on the surface. As O/C ratio increases, it is apparent that the plasma processing has high affinity for oxygen, which in turn would affect the electrical properties of the entire discharge when a yarn is immersed in the plasma due to increased oxygen abundance.

Future Work

Optimization of the plasma device in terms of input power to increase the plasma thermal energy and the ionization fraction to achieve higher electron number density (and consequently higher ion number density). This also includes conducting experiments at lower and higher frequencies to explore effect of changing frequency of the electric field on the treatment of yarns and filaments.

Conduct experiments using other reactive plasma gases, such as fluorocarbon gases CF4 and C3F6 to investigate the effect of plasma gas on the yarn treatment. Other gases to use are hydrocarbons, such as CH4, to develop enhanced deposition of carbon on the yarn surface and investigate the possibility of generating carbon-coated yarns with better lubricants and less frictional forces.

Conduct experiments on grafting cotton yarns with special chemicals, such as antimicrobial and insect repellant agents, to produce Biocidal yarns prior to weaving process.

REFERENCES

[1] Nicolas Gherardi, Gamal Gouda, Eric Gat, Andr´ e Ricard and Francois Massines, "Transition from glow silent discharge to micro-discharges in nitrogen gas", *Plasma Sources Sci. Technol*. 9 (2000) 340–346.

[2] S. Kanazawa, M. Kogoma, T. Moriwaki, and S. Okazaki, "Stable glow plasma at atmospheric pressure," *J. Phys. D. Appl. Phys*., vol. 21, pp 838-840, 1988.

[3] Nicolas Gherardi and Francoise Massines, "Mechanisms Controlling the Transition from Glow Silent Discharge to Streamer Discharge in Nitrogen" *IEEE Trans. Plasma Sci*. Vol 29. (3) pp. 536-544. (2001)

[4] Thomas Montie, Kimberly Kelly-Wintenberg, J. Reece Roth. "An Overview of Research Using the One Atmosphere Uniform Glow Discharge Plasma (OAUGDP) for Sterilization of Surfaces and Materials". *IEEE Trans. Plasma Sci*. Vol 28. No 1. Feb.

[5] Mounir Laroussi. "Nonthermal Decontamination of Biological Media by Atmospheric-Pressure Plasmas: Review, Analysis, and Prospects" *IEEE Trans. Plasma Sci*. Vol 30. No 4. Aug. 2002.

[6] J. Reece Roth, *Industrial Plasma Engineering,* Vol. 1: Principles, Institute of Physics Publishing, Bristol, UK, ISBN 0 7503 0318 2, 1995.

[7] H.H. Ngo, S.A. Vojta, J.A. Rohner, O.E. Hankins and M.A. Bourham, "Design and Parameter Measurements of an Atmospheric Pressure Plasma", 25th IEEE ICOPS, paper 3B03, Raleigh, NC, June 1-4, 1998, IEEE Cat.# 98CH36221, p.178, 1998.

[8] Brian Bures, Diagnosis and Application of Atmospheric Radio Frequency Glow Discharge Plasma, MS Thesis, North Carolina State University, 2001.

[9] M.G. McCord, Y.J. Hwang, Y. Qiu, K.L. Hughes and M.A. Bourham, "Surface Analysis of Cotton Fabrics Fluorinated in Radio-Frequency Plasma", Journal of Applied Polymer Science, Vol. 88, Issue 8, pp. 2038-2047, May 2003.

[10] Brian Chapman, Glow Discharge Processes, John Wiley & Sons, 1980.

[11] M. A. Liberman and A. J. Lichtenberg, Principles of Plasma Discharges and Materials Processing. New York: Wiley, 1994.

[12] Ph. Belenguer, J.P. Boeuf, Transition between different regimes of rf glow discharges, Phys. Rev. A 41 (1990) 4447–4459.

[13] Park J, Henins I, Herrmann H W, Selwyn G S and Hicks R F 2001 J. Appl. Phys. 89 20

[14] Gas breakdown in an atmospheric pressure radio-frequency capacitive plasma source Jaeyoung Park et al., J. Appl. Phys. 89, 15 2001

[15] A. Chirokov, A. Gutsol, and A. Fridman "Atmospheric pressure plasma of dielectric barrier discharges", Pure and Applied Chemistry, Vol. 77, No. 2 (2005), pp. 487-495.

[16] Chi-Ming Chan, Polymer Surface Modification and Characterization, Hanser/Gardner Publications, Inc., New York (1994).

[17] "Plasma and Antimicrobial Treatment of Nonwoven Fabrics for Surgical Gowns", Rajpreet K. Virk and Gita N. Ramaswamy (Kansas State University), and Mohamed Bourham and Brian L. Bures (N.C. State University), Textile Research Journal, Vol. 74 (12), pp. 1073-1079, December 2004.

[18] Cotton for Non-wovens: A Technical Guide.
(http:// www.cottoninc.com)

[19] "Surface Analysis of Cotton Fabrics Fluorinated in Radio-Frequency Plasma", M.G. McCord, Y.J. Hwang, Y. Qiu, K.L. Hughes and M.A. Bourham, Journal of Applied Polymer Science, Vol. 88, Issue 8, pp. 2038-2047, May 2003.

[20] D. Sun and K.G. Stylios, "Investigating the Plasma Modification of Natural Fiber Fabrics-The Effect on Fabric Surface and Mechanical Properties", *Textile Res. J.*, **75(9)**, 639 (2005).

[21] Belen Perez Rivera, Plasma-Aided Antimicrobial and Insect Repellant Finishing of Cotton, MS Theis, North Carolina State University, Raleigh, NC, 2006.

[22] "Modifying Nylon and Polypropylene Fabrics with Atmospheric Pressure Plasmas", M. G. McCord, Y.J. Hwang, P.J. Hauser, Y. Qui, J.J. Cuomo, O. Hankins, M.A. Bourham and L.K. Canup, Textile Research Journal, Vol. 72, No.6, pp. 491-498, June 2002.

[23] Abidi, N., Hequet, E., "Cotton Fabric Graft Copolymerization Using Microwave Plasma. I. Universal Attenuated Total Reflectance-FTIR Study", *Journal of Applied Polymer Science*, **93**, 145 (2004).

[24] Abidi, N., Hequet, E., "Cotton Fabric Graft Copolymerization using Microwave Plasma. II. Physical Properties", *Journal of Applied Polymer Science*, **98**, 896 (2005).

[25] "Surface Modification of Organic Polymer Films Treated in Atmospheric Plasmas", Yoon J. Hwang, Suzanne Matthews, Marian McCord and Mohamed Bourham, J. Electrochemical Soc., Vol. 151, No. 7, pp. C495-C4501, June 2004.

[26] Mao, J., "Durable Antimicrobial Finish for Cotton with New Technology", *AATCC Review,* **2(12)**, 15 (2002)

[27] "Polyvinyl Alcohol (PVA) Desizing Mechanism via Atmospheric Pressure Plasma Exposure", Suzanne R. Matthews, Marian G. McCord and Mohamed A. Bourham, J. Plasma Processes and Polymers, Vol. 2(9), pp.702-708, November 2005.

[28] J. Yip, "Low temperature plasma-treated nylon fabrics", *J. Mater. Process. Technol.*

[29] A.Bogaerts, E. N.Neyts, R.Gijbels, and J.van der Mullen, "Gas discharge plasmas and their applications," Spectrochim. Acta Part B, vol. 57, no. 4, pp. 609-658, April.**123** (2002), pp. 5–12

[30] M. Gheorghiu, F. Arefi, J. Amouroux, G. Placinta, G. Popa and M. Tatoulian. Surface Cross Linking and Functionalization of Poly(ethylene terephthalate) in a Helium Discharge. *Plasma Sources Science and Technology*, 6: 8-19, 1997

[31] D. Clark and A. Dilks. ESCA Applied to Polymers. XXIII. RF Glow Discharge Modification of Polymers in Pure Oxygen and Helium-Oxygen Mixture. *Journal of Polymer Science Part A-Polymer Chemistry*, 17: 957-976, 1979

[32] H.R. Griem, *Principles of Plasma Spectroscopy* (Cambridge University Press, 1997)

[33] NIST Physics Laboratory: Handbook of Basic Atomic Spectroscopic Data

(http://www.physics.nist.gov/cgi-bin/AtData/inesform)

[34] D.L. Book, NRL Plasma Formulary, Revised 2007

[35] Tom Dolan, Fusion Research: Principles, Experiments and Technology, in 3 volumes,

1982, available online at http://www.fusionnow.org/dolan.html